AIR FORCE INSTITUTE OF TECHNOLOGY

AIR UNIVERSITY
UNITED STATES AIR FORCE

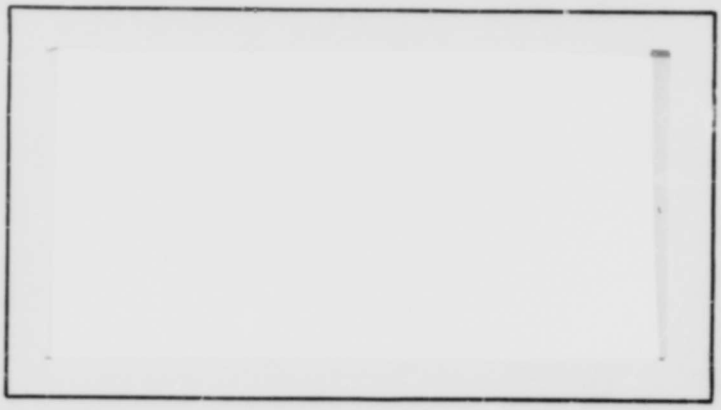

SCHOOL OF ENGINEERING

WRIGHT-PATTERSON AIR FORCE BASE, OHIO

AF-WP-O-MAY 62 3,500

EXPERIMENTAL STUDY OF A TRANSPIRATION-COOLED, WALL STABILIZED D-C ARC

Peter D. Tannen

GA/ME/62-6

GA/ME/62

EXPERIMENTAL STUDY OF A TRANSPIRATION-COOLED, WALL STABILIZED D-C ARC

THESIS

Presented to the Faculty of the

School of Engineering of the

Air Force Institute of Technology

Air University

in Partial Fulfillment of the

Requirements for the Degree of

Master of Science

By

Peter D. Tannen, B. Aero. Eng.

First Lieutenant USAF

Graduate Astronautics

August 1962

Preface

This study was undertaken with the hope that it would add significant information to the literature on electric arcs in forced convection. Although arcs have been used for many years, at present there is no one theory which can explain the various observed phenomena. Most major advances in plasma technology are based on empirical methods. Perhaps, when sufficient experimental information is available, a rigorous theoretical approach will be obvious.

Because of their extremely high operating temperatures, arc plasmas are difficult to contain within solid boundaries. Yet, it is the containment of these high temperature plasmas which makes them so useful to aerospace technology. Transpiration cooling, a method well known to rocket engine designers, is one possible way in which this confinement may be aided. The effects of transpiration flow on the electrical and heat transfer characteristics of a D.C. arc device are studied in this report.

This investigation was sponsored by the Aeronautical Research Laboratories, Office of Aerospace Research, Wright-Patterson Air Force Base, Ohio. I wish to thank Mr. Erich Soehngen for his ideas and suggestions which made this study possible. It has been a rewarding and an enjoyable experience to have worked for a man of his caliber. My thanks also to Mr. Kurt Daniels for his excellent job of design. I am grateful to Capt. D. Dye and Mr. E. Moore for their help in instrumenting and operating the device, and to Prof. M. E. Franke, my faculty advisor, for his suggestions. To all the members of my class, and to the personnel of the Aeronautical

Research Laboratories, I extend my sincere thanks for their contributions to this study. Particular mention must be made of my class mate, Lt. James R. Tedeschi, without whose patient assistance, I would never have completed this thesis.

I must also acknowledge a special indebtedness to my wife for maintaining our home and marriage in the face of extremely adverse conditions.

Peter D. Tannen

Contents

List of Figures

List of Symbols

Symbol		Units
A	Area	Ft^2 or cm^2
C_p	Specific heat of gas (0.124 for argon)	BTU/lb-°R
d	Arc diameter	cm
E	Column Voltage Gradient (= $V_{w/L}$)	Volts/cm
H_t	Rise in gas enthalpy	BTU/lb
h	Heat transfer coefficient	BTU/hr-ft^2-°R
I	Arc current	Amperes
j	Current density	Amps/cm^2
L	Distance between centers of top and bottom chambers	in., cm
$\dot{m}$	Total mass flow rate	lb/sec
N	Number of chambers	*
P_t	Total arc power	kw
P_c	Column power dissipated in wall region (P_c = I V_w)	kw
P_{Lt}	Total power lost to cooling water	kw
P_{Lw}	Power lost to cooling water in wall region	kw
q	Transpiration rate	lb/sec-ft^2
T	Temperature	°K, °R, °F
T_c	Gas temperature at inlet to porous segment	°R
T_g	Mean gas temperature in arc chamber	°R
T_w	Porous wall temperature	°R

Symbol		Unit
T_{in}	Cooling water inlet temperature	°F
T_{ont}	Cooling water outlet temperature	°F
T_{w1}	Cooling water temperature at wall inlet	°F
T_{w2}	Cooling water temperature at wall outlet	°F
V	Voltage	Volts
V_t	Total arc voltage	Volts
V_w	Voltage difference between centers of top and bottom chambers	Volts
W	Longitudinal mass velocity	$lb/sec\text{-}ft^2$
X	Distance along arc from cathode tip	in., cm
Q/W	Transpiration ratio	%
η_t	Device efficiency	%
	$= \frac{(P_t - P_{Lt}) \times 100}{P_t}$	
η_w	Wall efficiency	%
	$= \frac{(P_c - P_{Lw}) \times 100}{P_c}$	
σ	Electrical Conductivity	mhos/cm

Abstract

A study was made of a D-C arc device which confined the arc column within a 1/4-in.-diameter tube with transpiration-cooled walls. The tube was composed of individual porous segments, or chambers, which were electrically insulated from each other. The arc was struck between a tungsten cathode and a water-cooled, hollow copper anode. Argon was the principal gas used for the study, although two unsuccessful runs were made with helium. Except for one heat transfer experiment, all the gas entered the discharge region as transpiration coolant. Wall lengths of one, two, and three inches were tested at various transpiration rates.

The volt-ampere curves for this device had negative characteristics below 40 amperes and slope reversals in the range of 40-45 amperes. From this range to the maximum currents attained (190 amps), the arc voltage increased with increasing current for all wall lengths and gas flows. Simultaneous measurements showed that the arc column voltage gradient also had a positive slope with increasing current. Both the total voltage and the column voltage increased with increased gas flow.

The power lost to the external cooling water system was used to compute the device and wall efficiencies. The wall efficiency was based on the power lost in the wall region and the arc power dissipated in this region. Both efficiencies increased with higher flow rates at a constant power. For a given gas flow, both decreased with increased power. At the highest transpiration rates, device efficiencies on the order of 55%, and wall efficiencies of approximately 80%, could be maintained at the highest power levels.

The heat transfer coefficients for transpiration and non-transpiration flows were compared at low power inputs and at the same total mass flows. The results indicate that the coefficient may be reduced to 5% of its original value by the application of transpiration flow.

High-speed motion pictures at 7,000 frames-per-second were taken of the arc column, and the optical diameter of the column was used to compute the current density. The current density was then used to estimate the mean plasma temperature, which was approximately 13,000°K. High-speed photographs of the end view of the discharge failed to show an anode spot or any indication of spot rotation.

EXPERIMENTAL STUDY OF A TRANSPIRATION-COOLED, WALL-STABILIZED D.C. ARC

I. Introduction

Background

The needs of hypersonic flow research, materials testing, and space propulsion have pressed the development of high enthalpy gas heaters. One of the most satisfactory ways of obtaining the required enthalpies is by forced convection of electric arcs (Ref 1:4). Because of the size and weight of the power supplies necessary to run these devices, it is imperative that arc heaters for space applications be as efficient as possible (Ref 2:96). The long running time required of space engines further complicates the problem. This combination of high enthalpy, high efficiency, and continuous operation has been difficult, if not almost impossible to obtain (Ref 3:34).

The most common configuration for arc devices has the electrodes in a concentric arrangement (Ref 1:7). The gas flows through the annular gap between the electrodes, while the arc current passes across the gap. High power operation is generally associated with high currents and high thermal loadings. These cause electrode erosion, which results in gas contamination and short operating life. The erosion may be reduced by rotating the arc around the annulus. There are two primary methods for doing this:

1. Swirl the gas and rotate the arc by fluid forces (Ref 1:7; Ref 4:88).
2. Apply a magnetic field perpendicular to the arc current and rotate the arc by the resulting Lorentz force (Ref 5; Ref 6:22; Ref 7:3; Ref 8:4).

If the arc length is increased, then for a given current, arc voltage and power are increased (Ref 3:35; Ref 4:93). This is usually done by extending the outer electrode in the direction of gas flow, and allowing the arc to be "blown" to the required length (Ref 1:8; Ref 6:19). Strong swirl, or vortex, flow is often used to constrict and stabilize the arc (Ref 6:18; Ref 7:3; Ref 9:9). This type of gas flow allows sustained high power operation, but due to non-uniform gas heating (Ref 3:33) and strong secondary flows (Ref 4:89), some form of mixing or plenum chamber must be used (Ref 6:21; Ref 9:9). The heat losses to the plenum chamber may be quite high (Ref 9:19).

When the gas is injected without vortex motion the arc discharge tends to fill the cylindrical tube (Ref 4:85-87; Ref 6:18). These devices, called "wall-stabilized" arcs are generally more efficient than the "vortex-stabilized" types and are in wide use (Ref 3:33; Ref 6:21; Ref 8:3). However, at high power levels, the heat loss to the walls may be the major loss (Ref 10:222) and may in fact exceed 50% of all losses (Ref 6:23). Transpiration cooling has been suggested as a possible means of reducing this loss and protecting the walls (Ref 2:92; Ref 10:228).

Some work has been done in transpiration cooling of the positive electrode (Ref 3; Ref 11). These experiments primarily reduced electrode erosion, but the devices used were not high enthalpy heaters. This phase of arc work remains largely unexplored.

Theory

Wall cooling by fluid transpiration is effective for several reasons. First, the porous wall is cooled in a manner similar to a counterflow heat

exchanger (Ref 12:307). That is, the coolant moves through the porous wall from a cool exterior surface to a hot interior surface. This is opposite to the normal direction of heat flow in the wall. The second reason for the effectiveness of this type cooling is the direct injection of cool fluid into a hot gas flow. This cools the boundary layer (Ref 13:29) and transports heat from the wall into the main gas flow (Ref 12:462). The net result is that the film heat transfer coefficient is decreased, and the heat transfer to the wall is reduced. The effect is very pronounced and this reduction may be on the order of 55% for very low transpiration ratios (0.01), and up to 95% for higher ratios (0.05) (Ref 14:28, 29).

Most theoretical works (Ref 12:306; Ref 13; Ref 15) use the following assumptions:

1. Negligible heat transfer by radiation.
2. No heat loss through exterior surface of wall.
3. Coolant fluid leaves porous wall at wall surface temperature.

The heat balance equation that is developed on the basis of these assumptions may be rearranged to solve for the film coefficient (Ref 13:31; Ref 15:522):

$$h = \frac{\dot{q}\, c_p\, (T_w - T_c)}{(T_g - T_\infty)} \qquad (1)$$

Although there has been some question about the third assumption (Ref 14:4), it should prove valid for small pore sizes and thick walls. The second assumption is incorrect. However, if the heat lost per unit wall area is added to the basic heat balance equation, the film coefficient may be found

from:

$$h = \frac{\dot{q}\, c_p\, (T_w - T_c) + P_{Lw}/A_w}{(T_g - T_w)} \qquad (2)$$

Champion (Ref 16:346) states that radiation losses are about 0.1% of total arc power for a 1 atmosphere argon arc. However, Soehngen and Tedeschi at Aeronautical Research Laboratories, Wright-Patterson Air Force Base, stated in a personal communication that under certain conditions in an enclosed argon arc, radiation losses may be as high as 25% of total arc power. These losses are almost entirely absorbed by the walls. Equation (2) still holds, but the coefficient calculated is now the equivalent heat transfer coefficient (Ref 12:423). It is hoped that with strong transpiration flow a large fraction of this radiative loss will be fed back into the plasma.

The theory of high current arcs in forced convection is still being developed, and the general equations are solvable for only special cases (Ref 4:66-69; Ref 17:169). Even for the simple cases chosen there are large discrepancies between the theoretical model and the experimental device (Ref 4:69). For the low-current regime, there are several theoretical works now generally accepted (Ref 18; Ref 19). These studies predict negative volt-ampere characteristics. That is, decreasing arc voltage at increasing currents.

II. Experimental Objectives

The primary objectives of this experimental study are:

1. Operate a wall-stabilized, D.C. arc in argon at one-atmosphere, with all gas injected as transpiration coolant.

2. Obtain the electrical (V-I) characteristics of this device for different mass flows and various wall lengths.

3. Determine the arc column voltage gradient (E) for these same conditions.

In addition to the above it is hoped that the following (secondary) objectives will be attained:

4. Determine the efficiency of this device in converting electric power into gas enthalpy.

5. Operate the device without transpiration cooling for comparison purposes.

6. Extend the study to other gases, such as: helium, hydrogen, and nitrogen.

III. Description of Equipment

Introduction

Only the transpiration-cooled wall, which is the main component of the test device, is described in detail. The other components, instrumentation, and power supply are briefly described. Two complete devices were planned, one with a 1/4-in.-diameter inner wall, the other one with a 1/2-in.-diameter; all other dimensions were the same. Only the 1/4-in. device was completed in time for this study. A cross-section drawing of the 1/2-in. device is shown in Fig. 1. Fig. 2 is a photograph of the 1/4-in. arc device, while Fig. 3 shows an overall view of the experimental apparatus.

Cooled Wall

The porous wall was assembled from separate and independent sections (Fig. 4) which are referred to as wall sections or chambers. This unique design had several advantages which included:

1. Variation of wall length in 1/2-in. increments.
2. Simple replacement of damaged sections.
3. Incremental voltage drop could be measured by insulating the sections from each other.

Fig. 5 is a photograph of two chambers, one disassembled, the other assembled. The wall material was porous graphite NC-60 purchased from the National Carbon Company. This grade of graphite had a porosity of 48% and a mean pore diameter of 0.0013 in. The pore diameter was the smallest available and was chosen to ensure the smoothest and most uniform flow into the central (arc) region. The chambers were assembled by fitting the

graphite disk into the holder and soldering the cover plate in place.

Because of the difficulty in machining the porous material, it was hard to obtain a good gas seal between the graphite, the holder, and cover plate. As a result a large percentage of the flow diffused through the faces of the porous disk and escaped out the crack (Fig. 6). This sealing problem was complicated by the high temperatures expected and the desire to maintain good conductivity between the graphite and copper surfaces. The problem was solved by coating the faces of each porous disk with Saureisen "Conductalute" cement, and smoothing the surface with fine abrasive paper. In addition, a fillet of the same cement was built up at the inner radius of the crack (Fig. 7). This method of sealing was quite effective, and the seal was maintained even after long operating times.

An Iron-Constantan thermocouple was imbedded in one chamber as shown in Fig. 7. The junction was within 1/16-in. of the inner wall. This thermocouple and all others used in the experiment were electrically insulated from their surroundings by a sheath of Alphex shrinkable tubing. This material was slipped over each thermocouple and heated. The heating caused the tubing to shrink to about two-thirds of its original diameter and bond firmly to the thermocouple. The alphex material had a dielectric strength of 800 volts/mil. and increased the thermocouple time constant to about six-tenths of a second.

A straight length of 1/4-in. O.D. copper tubing formed the gas inlet to the internal gas manifold (Fig. 4 and Fig. 7). Another length of similar tubing was bent to fit the external shape of the chamber, as shown in Fig. 4. This tube provided water cooling for the exterior of the chamber.

The chambers were electrically insulated from each other by disks of artificial mica. This material is manufactured by the Minnesota Mining and Manufacturing Co., Inc. under the trade name of "Crystal-M" paper." Saureisen DW-30 cement was used to hold the insulation in place. This temperature resistant cement is electrically insulating, but heat conducting.

Electrodes

Anode. A water-cooled, hollow copper anode was used as this is a typical anode configuration for a wall-stabilized arc. The cooling water in the anode was directed by internal baffles as shown in Fig. 1. The upper portion of the anode acted as a support for the electromagnet described later.

Cathode. The cathode was a simple tungsten tip set in a copper water jacket (Fig. 1). Cooling water flowed up through the central tube, impinged on the bottom of the tungsten tip, and then flowed down and out through the outer passage. The cathode mounting plate had two gas inlets to allow gas to be blown into the arc longitudinally.

Both electrodes were held in place and centered by machined plates and threaded studs. These studs were insulated from the electrodes by fiber sleeves and washers.

Auxiliary Components

View Pieces. A 45-mm-diameter "Vycor" glass tube was mounted between the wall and cathode mounting plates (Fig. 1). This tube allowed the cathode portion of the discharge to be observed. Soft silicone rubber gaskets sealed the glass-metal interface so that an argon atmosphere could be maintained around the cathode.

A rectangular piece of "Vycor" glass placed in a machined brass piece was used as a window to view the arc column. Rectangular asbestos gaskets sealed the arc from the outside environment. Fig. 8 shows the view piece assembly and its position in the device. This window was installed only when it was desired to view the arc column.

Electromagnet. To prevent possible anode erosion and burnout, provision was made to rotate the anode spot. Magnetic field rotation was the means chosen to do this. An axial field of 300 gauss was produced by a direct current of 7.5 amperes in a coil of approximately two hundred turns of #14 enameled copper wire. The dimensions of this coil are shown in Fig. 9, while the position of the magnet on the apparatus is shown in Fig. 2. The coil was impregnated with DW-30 cement and wrapped with tape to ensure structural rigidity. The magnetic field strength was measured with a Bell, Inc. model 110 gaussmeter.

Instrumentation

Current. Arc current was read from a general purpose panel meter, converted to an ammeter by means of a 50-millivolt, 300-amp shunt. The meter face was marked as a dual range (0-300, 0-600 ampere) ammeter, and full scale deflection was produced by 37 mv. A calibration resistor was added in series so that the meter and shunt would be matched at full scale (50 mv, 300 amps). When checked against a laboratory standard, this ammeter was correct in the range 0 to 200 amps, and then read low by 1 amp for each additional 10 amps. At 300-amps (true) the meter read 290 amps. Since the

0-200 amp range was considered the most important for this experiment, the meter calibrator was set to read correctly in this range.

Voltage. The arc voltage was measured by means of a general purpose panel meter with a 5-milliamp full-scale deflection. A 30,000-ohm series resistor converted this meter to a 0-150-volt voltmeter. This meter had two scales (0-150 V, 0-300 V) marked on its face. The high scale was used by adding an additional 30,000-ohm resistor in series. A switch was added in parallel to this resistor so that the meter could be switched from high to low scale. This system was checked with a precision high-voltage power supply. The column voltage was measured with a Bruno-New York multimeter. The arc ammeter and voltmeter are shown in Fig. 10, while the electrical schematic is shown in Fig. 11.

Gas Flow. An Air Reduction Co., Inc. type 805-1601 argon dual-range flowmeter was used to meter the gas flow. This flowmeter had a range of 0-195 cubic feet per hour which was found to be accurate to within 5% at room conditions (1 atmosphere, 70-85°F). For higher gas flow rates, two of these meters were used in parallel to the gas line. A gas manifold (Fig. 3), supplied the gas to the individual wall sections. A thermocouple was mounted to this manifold so that gas inlet temperature could be measured.

Water Calorimetry. A schematic of the water calorimetry system is shown in Fig. 12. All water-cooled components were connected in series so that only one water flow measurement was needed. This measurement was made by passing the water through a Fischer-Porter #5 "Flowrator" (Fig. 13) for which a calibration curve was available in the laboratory. Four Harco "Thrift Therm TT-3Y" iron-constantan thermocouples were mounted

so that the water temperature rises for the whole device (Tin, Tout) and the wall region (T_{w1}, T_{w2}) could be measured. These thermocouples, and those previously mentioned, were connected to a Honeywell-Brown "Electronik Potentiometer Pyrometer." This Pyrometer (Fig. 14) was used in a range from 0 to 500°F.

Power Supply

Arc power for most runs was supplied by three A. O. Smith type A-3001-2 rectifiers attached in series (Fig. 15). Each unit had a maximum output of 40 volts at 300 amps, so the series arrangement permitted arc operation up to 120 volts at the rated current. For higher voltage operation an A. O. Smith type A-5000-10S rectifier was used. This allowed operation up to 500 amps at 250 V. The no-load and arc-on voltage ripples for the smaller rectifier are shown in Fig. 16.

The rectifiers had a minimum power output of about 3 kilowatts (kw) for the type 3001 and about 20 kw for the type 5000. In order to obtain lower power (lower current) various load resistors were used. Two water-cooled coils of stainless steel tubing, each having a resistance of 0.6 ohms, made up the first load bank. These dissipated about 1 kw at the current levels attained. For even lower currents, banks of quartz heat lamps were arranged in various series-parallel configurations. These heaters were Research, Inc. Radient Heating Units ALT 8-612. Each bank was capable of dissipating 24 kw at 440 V.

D.C. power for the electromagnet was supplied by a Perkins Engineering Co. power supply model M60 V. set at 28 V. The current to the magnet was regulated by means of a large variable resistor.

IV. Experimental Approach

Range of Variables

Wall Length. Data were obtained for four configurations of wall length, referred to as configurations A, B, C, and D, respectively. Configuration A was made up of two unsealed chambers and a chamber with a wall thermocouple. This assembly was primarily used to check the feasibility of the device, and test the instrumentation. The main series of tests were conducted using configurations B, C, and D, which consisted of two, four, and six chambers, respectively. All the chambers used in these configurations were sealed, and one chamber in each set had a wall thermocouple. Although the basic design can accommodate up to twelve chambers, power and water-cooling difficulties limited the scope of the investigation to a maximum of six chambers. Configuration E, consisting of two sealed and one thermocouple chamber was used for special investigations.

Gas Flow. Because wall length and thus area was variable, it was decided that the transpiration rate, Q (mass flow per unit area), would be a more basic parameter than total mass flow. The range of mass flow, transpiration rate, and longitudinal mass velocity are shown in Table I. It was felt that Q would have little meaning for the unsealed chambers, so total mass flow was used as the parameter for configuration A. An upper limit on flow rate was set by compressibility effects due to arc heating. A sample of the raw data obtained is shown in Table II.

Current. The current was varied from a low of 10-15 amps to approximately 100 amps. Configuration D was not run at currents below 30-35 amps since the ballast resistors were not large enough to "load" the power unit (A-5000) below this range. The upper limit on current varied with configuration and gas flow rate, but was determined by one or more of the following:

1. Arbitrary wall temperature limit of 450°F.
2. Local boiling of anode cooling water.
3. Insulation failure.

The maximum current attained was 190 amps at a transpiration rate of 1.013 lb/sec-ft^2 using configuration B. This also corresponded to the maximum power reached (15.6 kw).

Gas Type. Argon was the primary gas selected for this study due to its ease of ionization and low heat conductivity. Because argon is inert and monatomic, arcs struck in this gas are more easily analyzed than in other gases. Some runs were attempted with helium, but these ended abruptly due to arc instability and insulation failure. Although the wall could normally be maintained at relatively low temperatures, there was a possibility of insulation failure which could result in "arc-over" to the porous segments and subsequent high local temperatures. Since nitrogen and carbon react at high temperatures and can produce a deadly gas, no runs were attempted with nitrogen.

Non-Transpiration Flow. Some comparative data were obtained using configuration E. These runs were restricted to low arc currents due to wall overheating and insulation failure at currents above 30 amperes.

Procedure

Starting. The arc was usually started by inserting a carbon rod down through the anode and chamber region until contact was made between cathode and anode. The rod was then withdrawn drawing the discharge with it When the end of the rod passed the anode, the arc would stabilize on the anode. A high gas flow was needed to start the arc. Starting was also aided by allowing some argon flow to enter the discharge region through the cathode inlets. For configuration D, this starting method was unsatisfactory. Due to the high flow rates required to start the arc, the carbon rod could not be held in the apparatus. Instead, a fine wire was inserted between the cathode and anode before the gas and power were turned on. When the power was applied the wire vaporized and provided a conducting path for the plasma. The major disadvantage of this method was that the exploding wire left a deposit on the interior surfaces of the device, even though a high gas flow was maintained.

Volt-Ampere Characteristics. The current was varied by adjusting the manual control on the power supply. Since this was a time-consuming task, arc voltage readings were taken while varying over the range of gas flow at each current setting. In this manner a complete set of data could be obtained with one traverse of the current range. Usually, data were taken first at the highest flow rate and then at decreasing rates. This was done so that the region of high wall temperature and insulation failure, which occurred at low flow rates, could be approached cautiously. In the low-current regime, the current was dependent on the external load resistor, therefore, the apparatus had to be shut down to change this resistance.

Column Voltage Gradient. The voltage measured for the column voltage gradient was the potential difference between the top and bottom chambers. Since each chamber was 1/2-inch thick, there was some uncertainty as to actual column length to which this voltage could be referenced. Because carbon is a fairly good conductor, the distance between disk centers was used as the reference length. Arc voltage distribution measurements were made on a configuration consisting of three sealed chambers. The total length of the arc was undetermined due to the long (2-in) anode. No definite anode spot trace was observed.

Heat Transfer Data. The total arc power was determined from total arc voltage and current. The arc column power was calculated from the column voltage drop and arc current. This latter power is more correctly termed the power dissipated in that portion of the column between centers of the top and bottom chambers. Total power loss was found from the water flow rate and temperature rise. The temperature rise of the water flowing past the wall region was also measured, and the power lost through the walls was calculated. The total arc power and the device losses were used to calculate the device efficiency as defined in the List of Symbols. Similarly, the column power and wall losses were used to calculate a wall efficiency. The wall temperature and gas inlet temperature were also recorded.

Photographs. Fastax (7,000 frames per second) movies were taken of the arc column so that an estimate of the arc diameter could be made. Fastax movies were also made looking along the arc column in an attempt to observe arc stability and rotation. These films are available at the Thermo-Mechanics Research Laboratory of the Aeronautical Research Laboratories.

V. Discussion of Results

Operation of the Device

In general, the device was reliable and simple to operate. The major difficulties noted were insulation failure and anode over-heating. These would occur at various combinations of high power and low gas flow. For configuration D, high transpiration rates required high total flow rates. When heat is added to a compressible fluid in a duct, an additional pressure drop is needed to maintain a constant mass flow rate. Since the exit was open to the atmosphere, this additional pressure drop could be supplied only by increasing the inlet pressure. Due to the limited inlet pressure available from the flow meter, high flow rates were not obtainable for configuration D with the arc on. An investigation of the longitudinal pressure distribution within the arc would be of considerable interest.

Volt-Ampere Characteristics

Figures 18 through 21 show the volt-ampere characteristics of the four configurations as functions of gas flow rate. As previously mentioned, total mass flow was used as the parameter for configuration A, while transpiration rate was the parameter chosen for configurations B, C, and D. Data for five flow rates for configuration B and two flow rates for C were not plotted on their respective figures in order to preserve clarity. These data show the same trends as those plotted and are available from the author.

The significant increase in arc voltage with increasing gas flow, at a constant current, has been previously found by other experimenters (Ref 1:8; Ref 3:100). The low-current characteristics are negative at a constant gas flow. This was predicted from low-current theory (Ref 17; Ref 18; Ref 19). For most arc devices, the voltage continues to decrease, or at most remain constant, as the current is increased (Ref 1:8). For all configurations except D, and all flow rates tested in this study, the volt-ampere curves had minimums at approximately 40 amperes. As the current was increased beyond 40 amps, the slope reversed and the voltage increased. This positive slope of the characteristic curve has been noted in other arc devices (Ref 3:17-23, 130-132), but it was related primarily to an increase in anode fall voltage. In the present study, the positive characteristics appear to be related to corresponding increases in arc column voltage gradient. This is discussed in more detail in the following section. Because of the previously mentioned difficulties of load bank adjustment and starting, configuration D was not run at low currents.

Arc Column Voltage Gradient

The column voltage gradient for configuration A was measured for only one gas flow rate and is shown in Figure 22. The variation of voltage gradient as a function of arc current and transpiration rate is shown for configurations B, C, and D in Figures 23, 24, and 25 respectively. For these configurations, at a constant current, the gradient increased with increasing transpiration rate. For a given flow rate, the column gradient increased as the current was increased. This appears to be true over the entire current range.

This behavior may be explained if we can assume that the majority of the current was carried by a well-defined, conducting column. This assumption is typical of arc work and is generally sound (Ref 1:8; Ref 20:331). The following form of Ohm's Law will also be used:

$$V_w = IR_c \tag{3}$$

where R_c is the column resistance in ohms. For each configuration, the reference column length was a constant, so that the linear increase of voltage gradient with current, as shown in the figures actually indicates a linear increase of column voltage . This linear change of voltage with current indicates a constant resistance, which itself indicates a fairly constant plasma temperature, since arc resistance decreases with increasing temperature. It has been postulated that for argon at one atmosphere, the radiation losses are proportional to the 7.2 power of temperature (Ref 20:9). This seems to be due to the strong dependence of emissivity on temperature. If this is true, then large increases in arc power density caused by increased current may be dissipated by the increased radiation losses without causing an appreciable rise in arc temperature.

When the flow rate was increased the column gradient also increased. This indicates that the outer periphery of the conduction column was being increasingly cooled and the arc was constricted to a smaller diameter. As a partial check of the above theory a separate experiment was performed. Fastax motion pictures were taken of the arc column for different transpiration rates. The results of this experiment are shown in Table III. The arc

diameter could be estimated from the photographs, and used to compute the current density, j. The following form of Ohm's Law was used to compute the conductivity:

$$j = \sigma E \tag{4}$$

The electrical conductivity, σ, is a known function of temperature (Ref 4:174) so that the mean plasma temperature could be computed. It should be noted that the apparent arc diameter did decrease when the transpiration rate was increased. A lower bound on arc temperature was established by assuming that the conduction column completely filled the inner diameter, and then using this diameter for the computations. This portion of the study ought to be extended to higher currents in order to verify the above theories. The temperatures found are in the range of strong argon radiation.

Figure 26 shows the voltage distribution of the arc for configuration E at three transpiration rates and at a current of approximately 45 amps. This study was performed in an effort to determine whether the column gradient varied along the length of the arc. It had been postulated that the gradient might be maximum at the lower chamber and decrease in the region of the upper chambers. This theory was based on the fact that the effects of the transpiration cooling should be strongest at the lower chamber.

However, the data obtained seem to indicate that the gradient was constant throughout the transpiration-cooled region. In fact it appears that the voltage gradient for the lower portion of the discharge is much less than for the remainder of the column. The lower region of the arc was probably not constricted, since there was no gas flow.

The potential difference between the cathode and the wall mounting plate approximates the cathode fall voltage, due to the close proximity of these two components, and the low column gradient in this region. This value (8-9 volts) agrees with previously measured values of this quantity (Ref 21:300). The horizontal lines at 65, 82. and 97 volts represent the anode potentials for the respective transpiration rates. These potentials were constant over the length of the anode. An anode fall of 6 volts was assumed so that an estimate of the total arc length could be made. The constant gradient lines were extended to a point 6 volts below the anode potential. As shown in Figure 26, the total arc length found by this method is approximately the same for the different flow rates.

Device Efficiency

As shown in Figures 27 through 30, at a constant arc power, the device efficiency increased with increasing gas flow. This trend is probably due to the lowering of the mean gas temperature, thereby decreasing the heat loss to the wall and cooling water. As the total arc power was increased the device efficiencies decreased. However, the drop in efficiency was less rapid for the higher gas flows. In fact, at the highest transpiration rate used, the efficiency was nearly constant for the entire range of arc power (Figure 28). Since the device as a whole was not designed for maximum efficiency, it should not be compared to commercial arc heaters.

Figures 31 and 32 show the division of power losses among the major components for two transpiration rates. For both transpiration rates, the largest single loss was at the anode. The per cent loss to this component was constant for the high gas flow, but increased with power at

the lower flow rate. An additional thermocouple would be needed to separate the cathode losses from those to the wall mount. The fact that there was no gas flow over these two components probably contributed to their high combined heat loss. In fact, the voltage distribution shown in Figure 26 indicates that the discharge may nearly fill the inner diameter in this section. This would certainly produce increased losses to the mount plate.

The increase in total heat loss with increased power appears to be associated with the increasing wall loss. This loss rises more rapidly for the low transpiration rate. The next section discusses the wall losses in more detail. All heat losses shown in Figures 31 and 32 are in per cent of total arc power.

Wall Efficiency

Rather than show wall losses as functions of total arc power, the wall efficiencies are plotted against the arc column power. Column power was chosen since this is the part of the arc power that is dissipated in the transpiration region. The two thermocouples needed to measure wall losses were not installed on configuration A. Figures 33, 34, and 35 show the wall efficiencies as functions of column power and transpiration rate for configurations B, C, and D. The curves for the five transpiration rates of configuration D were very close to each other, so only two representative rates are plotted in Figure 35.

The curves roughly tend toward 100% efficiency at zero power. This is due to the decreased losses at low power levels. A similar tendency was not noticed for the total arc efficiencies (Figures 27 through 30)

since the anode and cathode losses were approximately constant percentages of total arc power for the range tested (Figures 31 and 32). Figures 33 and 34 show the increased wall efficiencies with increased transpiration rate. This effect diminishes as the higher transpiration rates are approached. However, it should be noted that the wall efficiencies at the higher rates do not drop as rapidly with increased power as the efficiencies at the lower rates. For all rates, the drop in efficiency is probably due to the higher gas temperatures which occur at the higher power levels.

Gas Enthalpy and Performance

Although the device was not designed for maximum enthalpy, the gas enthalpy rise was of considerable interest. Figures 36 through 39 are plots of the gas enthalpy rise as a function of total arc power and gas flow. For a constant flow rate, enthalpy increased with rising arc power, while for constant power it increased with decreasing gas flow. However, at the lower transpiration rates, the curves are quite close, and even appear to cross (Figures 37 and 38). This is definitely related to the low efficiencies recorded for these flow rates. That is, for a given power in the gas, the specific enthalpy will increase with decreasing gas flow. But for this device, the conversion efficiencies were very low for the low flow rates (Figures 28 and 29). Therefore, for a given arc power, the power actually going into the gas stream was lower for these rates. The net result was that the specific enthalpy did not increase significantly when the transpiration rate dropped below approximately 0.20 $lb/sec\text{-}ft^2$.

Figures 40 through 43 are cross-plots of the gas enthalpy and device efficiency curves. From the first three of these figures, it appears as

though the device tends toward the same limiting efficiency of 60% for all gas flows, at zero enthalpy. Note also that for low transpiration rates the high enthalpies are associated with low efficiencies, and that, in general the high flow rates maintained their high efficiencies even for high enthalpies. The performance curves for configuration D (Figure 43) behave differently from those of the other configurations by tending toward a constant efficiency of 50% at high enthalpies. The reason for this behavior is not known.

Heat Transfer Comparison

As mentioned in Section IV, the non-transpiration flow study could be made only at low currents due to wall overheating. No attempt was made to obtain volt-ampere or voltage gradient curves because of the high wall temperatures. Three different mass flows were used in strictly axial (non-transpiration) flow, then three comparison runs were made using the same mass flows in the transpiration mode. The total arc power was maintained at approximately the same level for the six runs. The results are shown in Table IV. The gas temperatures were computed from the enthalpy rises. Equation 2, page 4 was used to compute the equivalent heat transfer coefficient. The results presented in this table clearly show that transpiration cooling greatly reduced the heat transfer coefficient. This reduction may even increase at higher currents, since low wall temperatures and low wall losses could be maintained with transpiration cooling.

Variation of Gas Type

Two runs using helium were attempted. The first lasted about two minutes and ended when the insulation failed. Total arc voltage was

considerably higher than for a similar argon arc. The plasma flame was very long and appeared transparent. This run resulted in the distruction of two chambers. The second attempt confirmed the observations of the first. In addition, the flame seemed to be a red-green color rather than the brilliant white usually seen with argon. This attempt ended because of recurrent instability of the arc.

Accuracy of Results

Arc voltage and current could be determined within 1 volt or 1 ampere. Column voltage was accurate to 0.5 volt for readings below 45 volts, and within 1 volt above that level. Temperature could be read to the nearest degree fahrenheit. However, it should be noted that at the water flow rates required to keep the anode cool, the temperature rise in the wall region was on the order of only 2-3°F. This was generally the case at low power levels and high transpiration rates. The water flow could be determined with an accuracy of 0.001 lb/sec. The gas flow meter was read to within 1 ft^3/hr. with an accuracy of ± 5%. All computations were done on a desk calculator, and the results were reduced to three significant figures, except for special cases where the additional accuracy was warranted.

In general, individual runs could be reproduced within ± 3%.

VI. Conclusions

1. The device was reliable and simple to operate. It should prove to be a useful tool for further arc research.

2. The positive volt-ampere characteristic curves are due to the positive slope of the column voltage gradient curves.

3. The positive slope of the column voltage gradient appears to be due to the cooling and constricting effect of the transpiration flow.

4. The column gradient is constant within the transpiration-cooled region.

5. High enthalpies can be attained at good device efficiencies and high transpiration rates.

6. Transpiration flow is a very effective method of decreasing heat losses to a confining wall although a large fraction of those losses may be due to radiation.

VII. Recommendations

Equipment Changes

1. Provide separate water cooling to the anode and to the wall region. Large flow rates are needed to cool the anode, while small flow rates are required in the wall region for accuracy of measurement.

2. Redesign the anode to provide better cooling.

3. Increase the diameter of the central hole in the wall mount plate. This would allow the cathode to be raised into the vicinity of the bottom chamber, and should minimize the cathode and mount plate losses.

4. Manufacture the porous disk from some material other than carbon; possibly porous alumina or zirconia. This would allow the experiments to be extended to nitrogen.

5. Use a resistance bank which is more easily varied than the quartz heat lamps.

6. Provide a better means of starting the long configurations; e.g., high frequency starter.

Experimental Extensions

1. Determine the flow rate to each chamber.

2. Vary the transpiration rate along the length of the arc in order to optimize efficiency and enthalpy.

3. Extend the study to longer arc lengths and to the 1/2-inch inner diameter design.

4. Run the arc with mixed axial and transpiration flows to determine the effect of the ratio of transpiration to axial flow.

5. Extend the study to other gases.

6. Determine the radiation losses from the arc column.

7. Measure the axial and radial temperature and pressure variations within the plasma.

8. Design a transpiration-cooled anode and determine its effects on the arc characteristics.

9. Measure the velocity and enthalpy distribution within the device, and in the plasma flame.

Analytic Extensions

1. Set up and analyze a simple model incorporating diabatic flow in a constant area duct, modified to include constantly increasing mass flow.

2. From the temperature, pressure, and velocity distributions make an estimate of the heat transfer rates. Compare the computed rates with the measured rates.

Bibliography

1. John, R. R. and W. L. Bade. "Recent Advances in Electric Arc Plasma Technology." ARS Journal, 31:4-17 (January 1961).
2. Ehricke, K. A. "Comparison of Propulsion Systems," in Advanced Propulsion Systems Symposium, edited by M. Alperin and G. P. Sutton. New York: Pergamon Press, Inc., 1959, p.p. 71-104.
3. Sheer, C., et al. Effect of Fluid Transpiration Through the Anodic Arc Boundary. Aeronautical Research Laboratory Contract AF 49(648-477). West Orange, New Jersey: Vitro Laboratories, June 1961.
4. Cann, G. L. Energy Transfer Processes in a Partially Ionized Gas. Doctoral Dissertation. Pasadena, California: California Institute of Technology, 1961.
5. Christensen, D. and R. D. Butler, Ph.D. Arc Jet Tunnel Development and Calibration for Parabolic Re-Entry Simulation. Final Report AEA Contract No DA-04-495-506-Ord-1872. Santa Anna, California: Plasmadyne Corporation, 1961.
6. Greer, E. H. Investigation of the Electrical and Heat Transfer Characteristics of a Magnetically-Rotated D-C Arc Between Cooled Metal Electrodes. Unpublished Thesis. Dayton, Ohio: Air Force Institute of Technology, Wright-Patterson Air Force Base, 1960.
7. Eschenbach, H. C. and G. M. Skinner. Development of Stable, High Power, High Pressure Arc Air Heaters for a Hypersonic Wind Tunnel. WADD Technical Report 61-100. Dayton, Ohio: Wright Air Development Division, Wright-Patterson Air Force Base, 1961.

8. Shepard, C. E. and D. R. Boldman. Preliminary Development of Electrodes for an Electric-Arc Wind Tunnel. NASA Memo 4-14-59E. Washington, D. C.: NASA, 1959.

9. Skifstad, J. G. A Study of Thermal Arc-Jet Propulsion. Report I-61-2, ONR Contract Nonr 1100(17). Lafayette, Indiana: Purdue University, 1961.

10. Carmac, M. "Plasma Propulsion Devices," in Advances in Space Sciences, Vol. 2, edited by F. Ordway, III. New York: Academic Press, Inc., 1960, pp. 215-262.

11. Schoeck, P. A. and E. R. G. Eckert. "Experiments on the Transpiration Cooled Anode of an Electric Arc," in Proceedings of the 1961 Heat Transfer and Fluid Mechanics Institute, edited by R. C. Binder, et al. Stanford, California: Stanford University Press, 1961, pp. 193-207.

12. Eckert, E. R. G. Heat and Mass Transfer (Second Edition). New York: McGraw Hill Book Company, Inc., 1959, pp. 301-310, 456-463.

13. Yuan, S. W. and A. Barszotti. "Experimental Investigation of Turbulent Pipe Flow with Coolant Injection," in 1958 Heat Transfer and Fluid Mechanics Institute. Stanford California: Stanford University Press, 1958, pp. 25-39.

14. Lenoir, John M. Hot Wire Apparatus for Measurement of Transpiration Effects on Heat Transfer Coefficients. Jet Propulsion Laboratory Progress Report No. 20-300. ORDCIT Contract No. DA-04-495-Ord 18. Pasadena, California: California Institute of Technology, 1956.

15. Wheeler, H. L., Jr. and P. Duwez. "Heat Transfer Through Sweat Cooled Porous Tubes." Jet Propulsion, 25:519-524 (1955).

16. Champion, K. S. W. "The Theory of Gaseous Arcs: II, The Energy Balance Equation for the Positive Column." Proc. of the Physical Society, B65:345-356 (1952).

17. ---------- "The Energy Balance Equations for the Positive Columns of High Pressure Arcs." Proc. of the Physical Society, B66: 169-174 (1955).

18. Suits, C. G. "High Pressure Arcs in Common Gases in Free Convection." Physical Review, 55: 561-567 (1939).

19. Suits, C. G. and H. Poritsky. "Application of Heat Transfer Data to Arc Characteristics." Physical Review, 55:1184-1191 (1939).

20. Grey, J. Heat Transfer From an Ionized Gas to a Gaseous Coolant. Proposal for an extension of work initiated under ONR Contract Nonr 1858(31). New Jersey: Princeton University, 1962.

21. Cobine, J. E. Gaseous Conductors. New York: Dover, 1958.

Figures 1 through 43

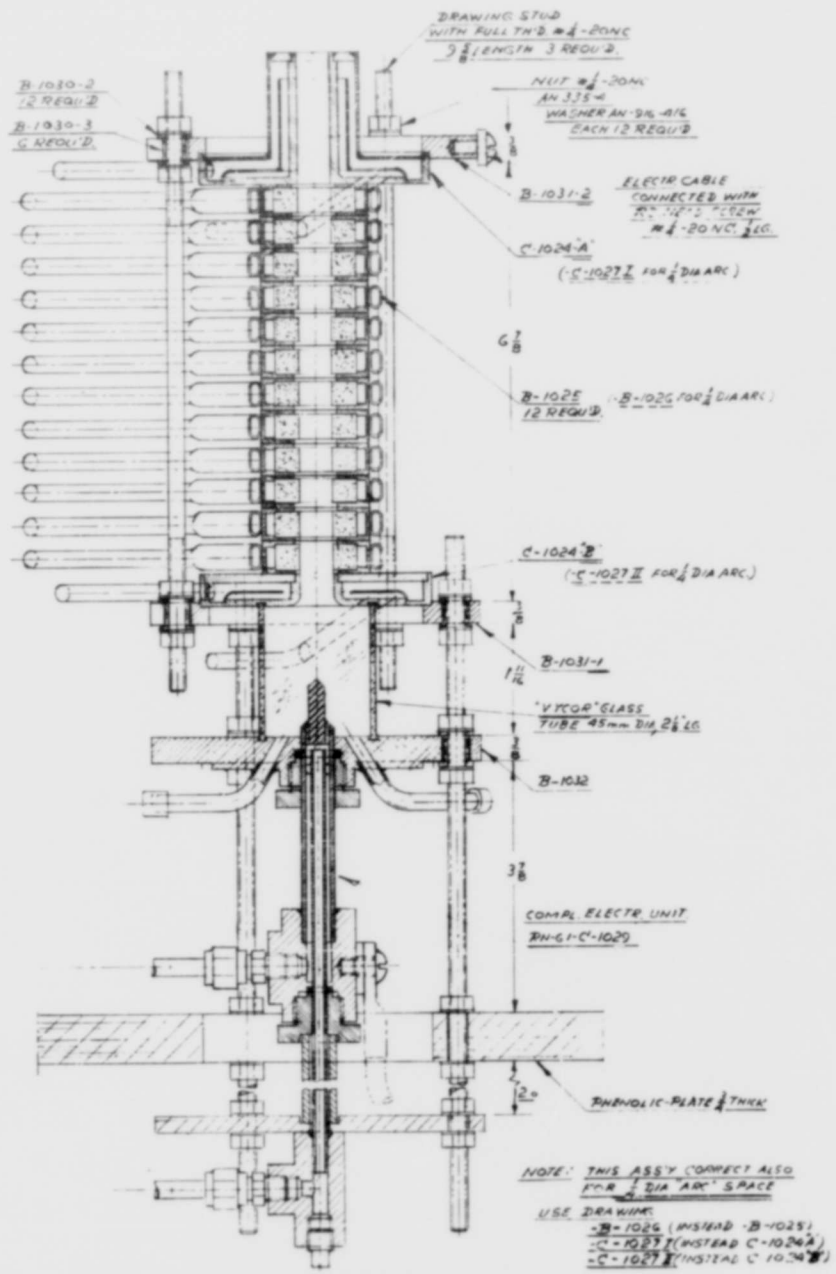

FIGURE 1

CROSS-SECTION OF ARC ASSEMBLY

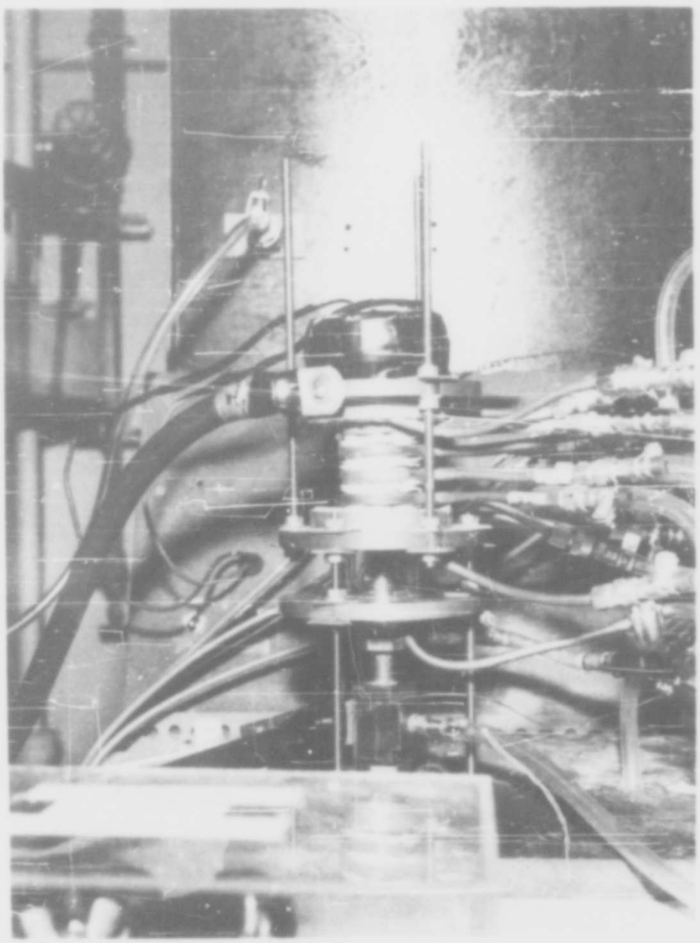

FIGURE 2

FOUR-CHAMBER CONFIGURATION

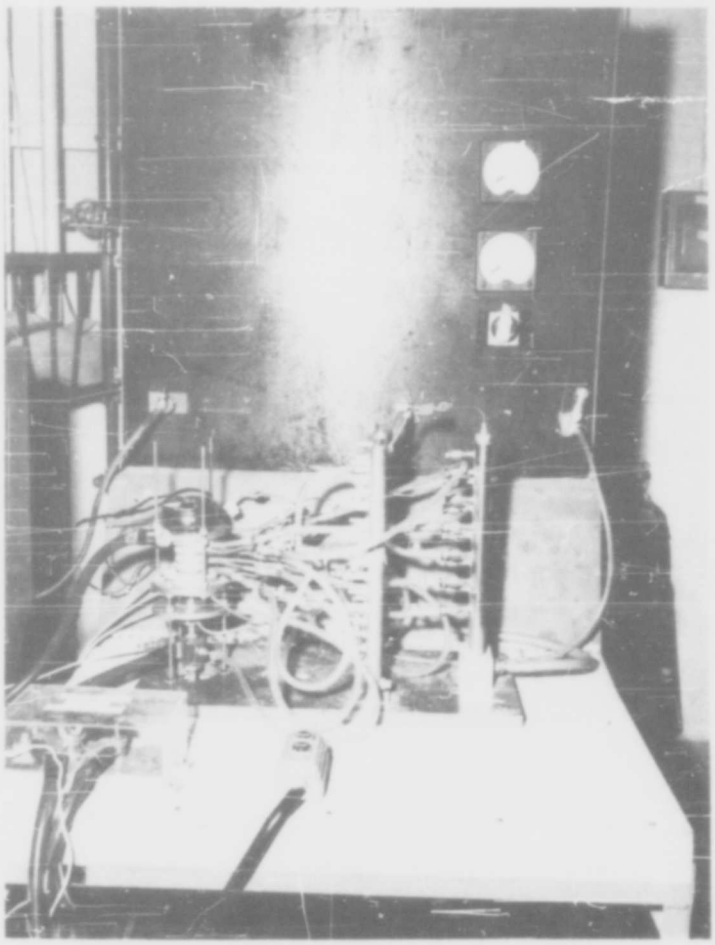

FIGURE 3

ARRANGEMENT OF APPARATUS

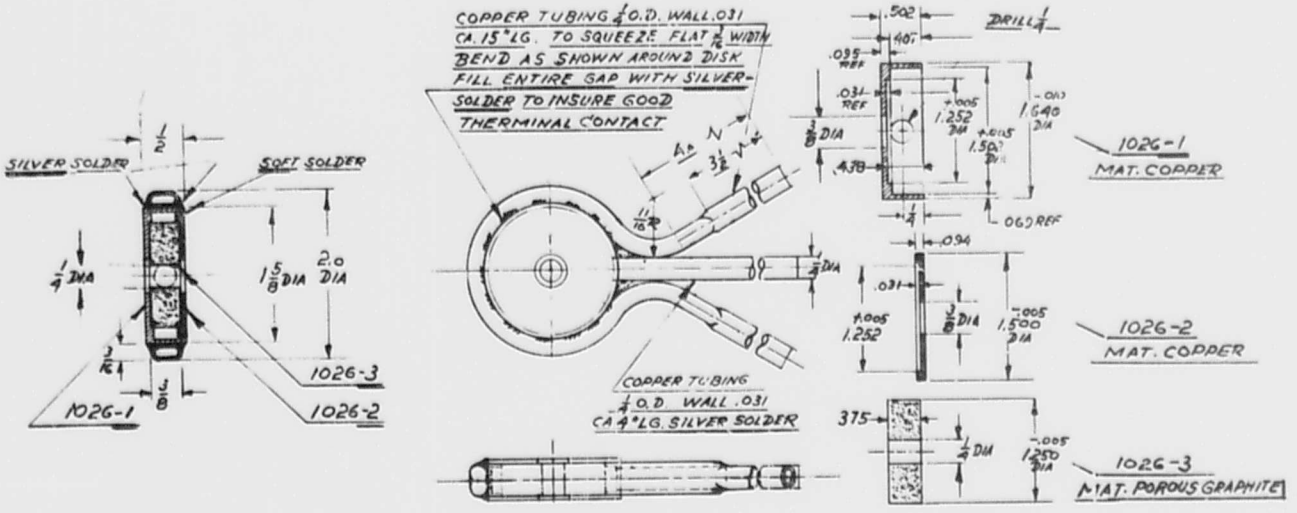

FIGURE 4

ENGINEERING DRAWING OF CHAMBER ASSEMBLY

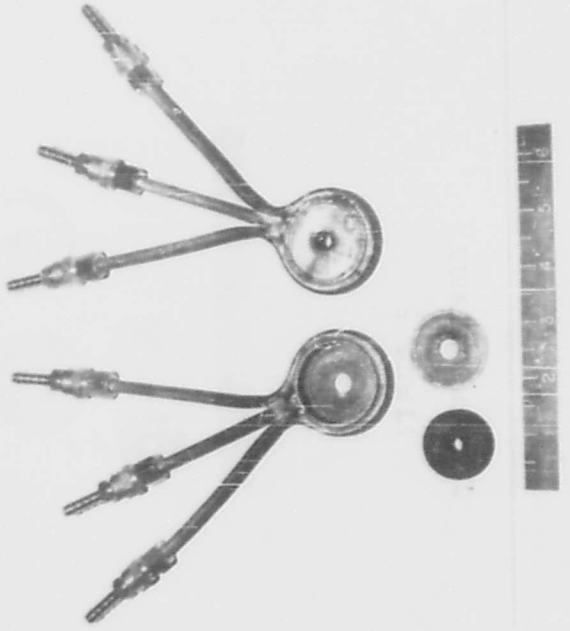

FIGURE 5

CHAMBER ASSEMBLY

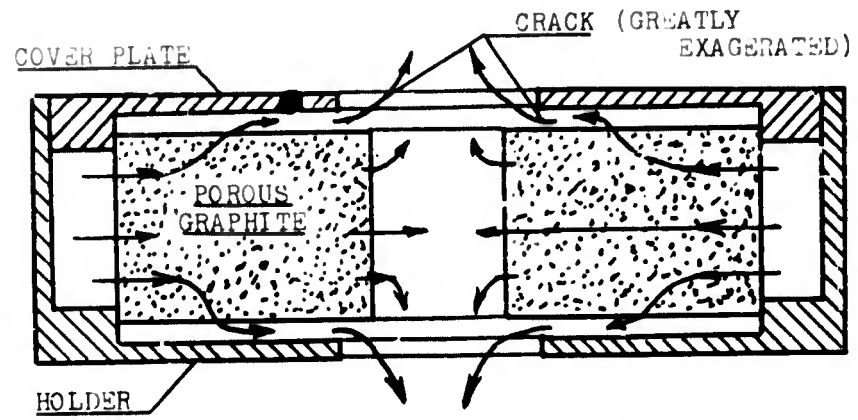

FIGURE 6

CHAMBER GAS FLOW BEFORE SEALING

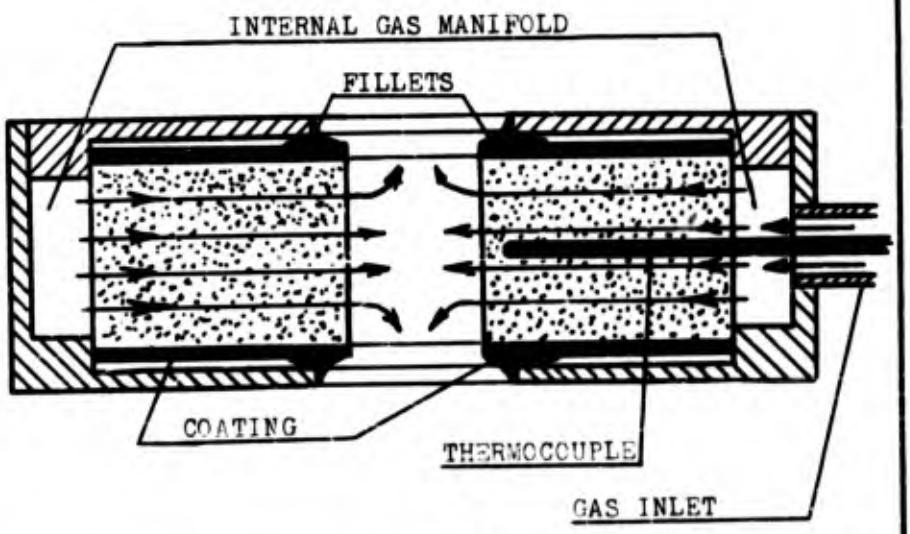

FIGURE 7

CHAMBER ASSEMBLY WITH WALL THERMOCOUPLE AFTER SEALING

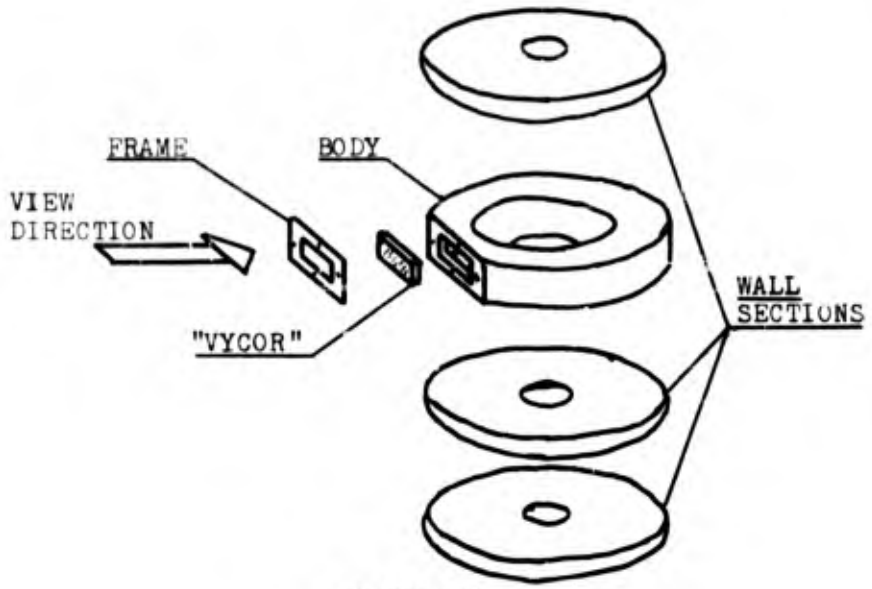

FIGURE 8

ARC COLUMN VIEW PIECE

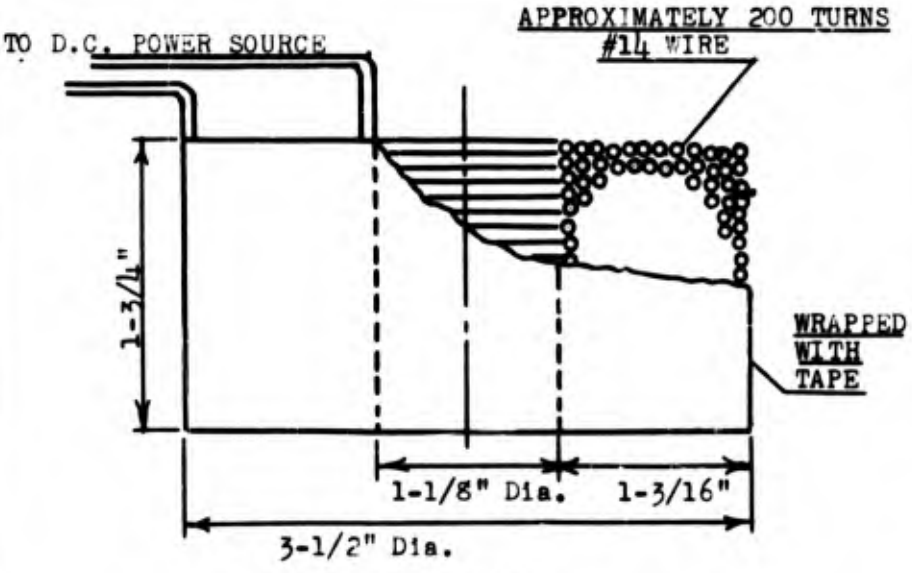

FIGURE 9

ELECTROMAGNET

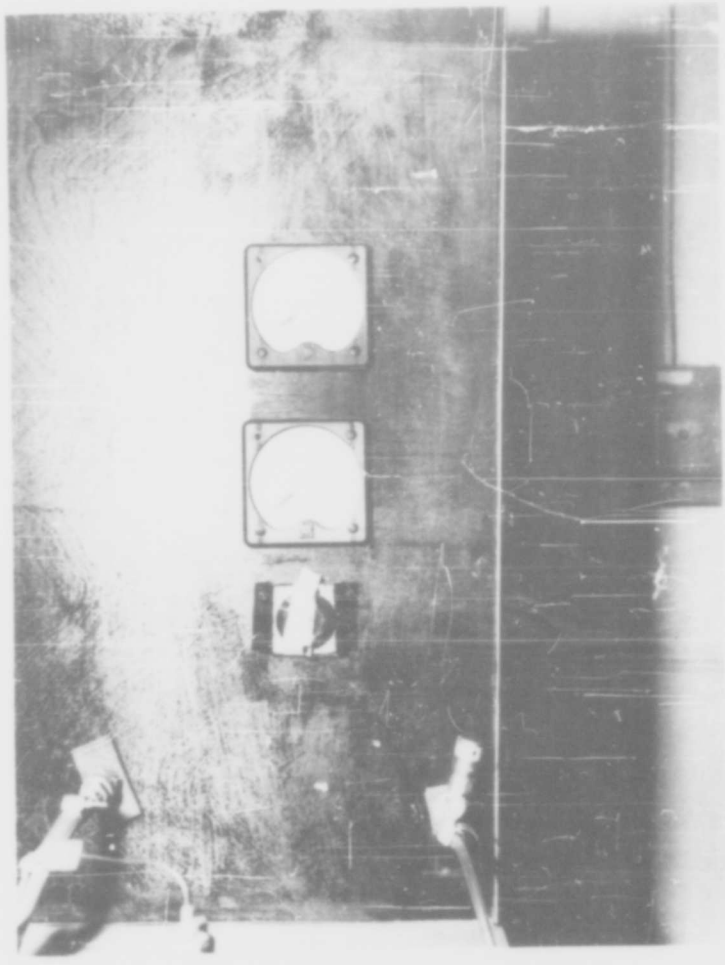

FIGURE 10

ARC VOLTMETER AND AMMETER

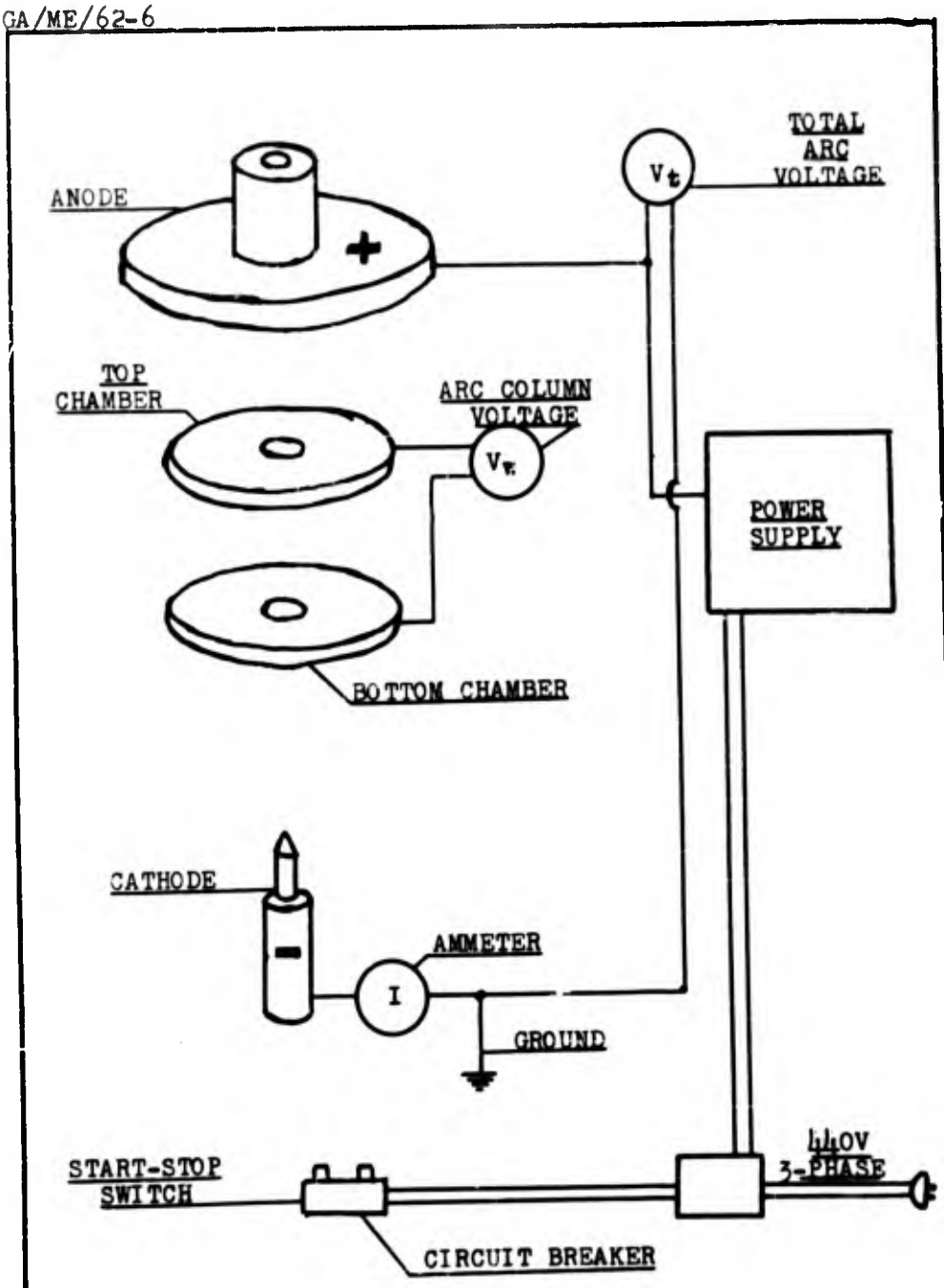

FIGURE 11

SCHEMATIC OF ARC ELECTRIC SYSTEM

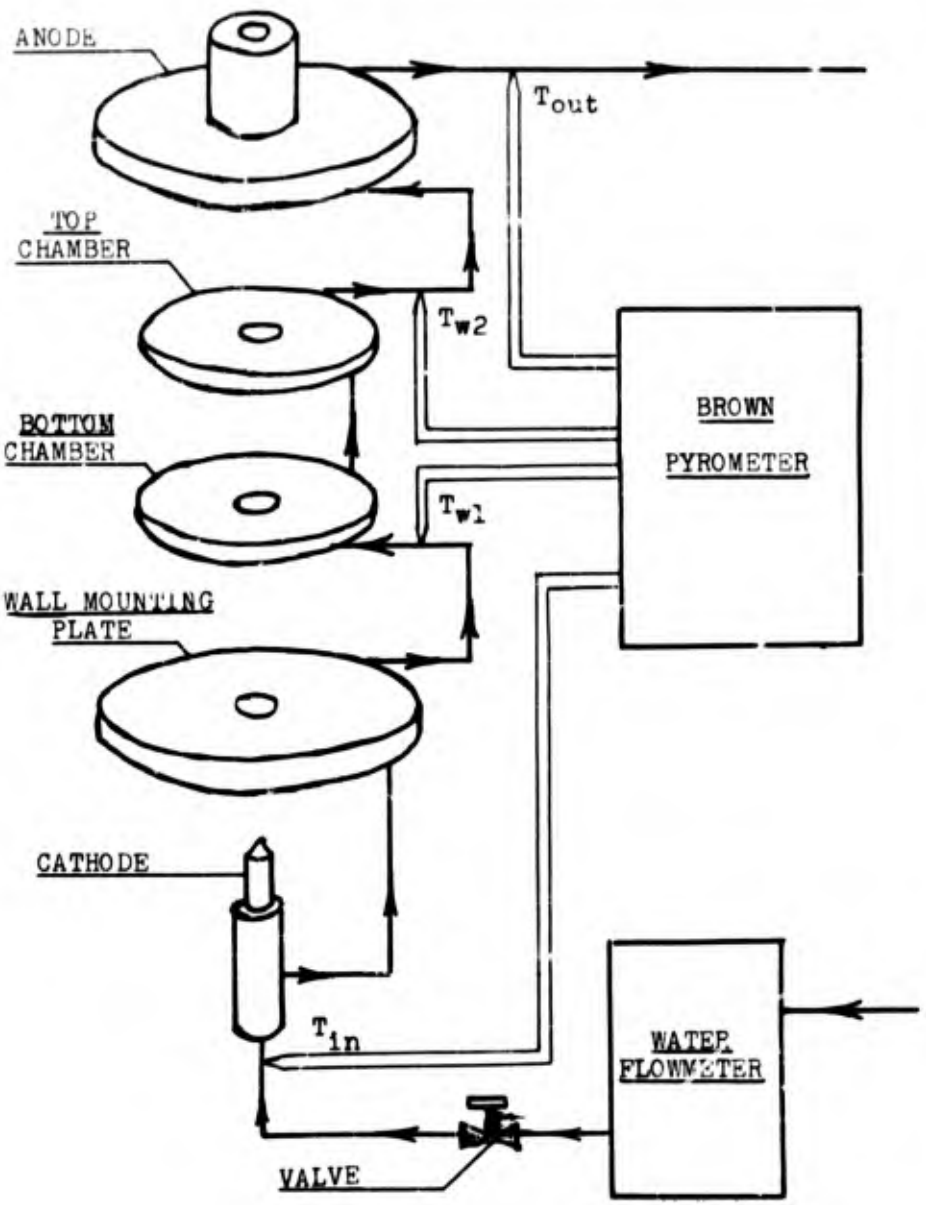

FIGURE 12

SCHEMATIC OF WATER CALORIMETRY SYSTEM

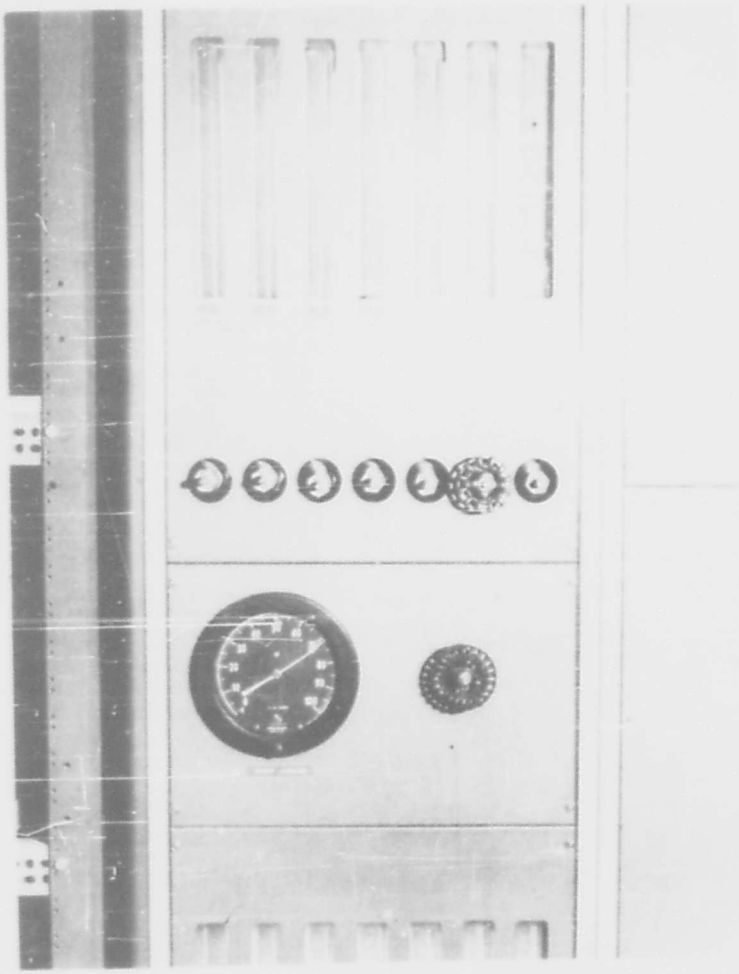

FIGURE 13

WATER FLOWMETER

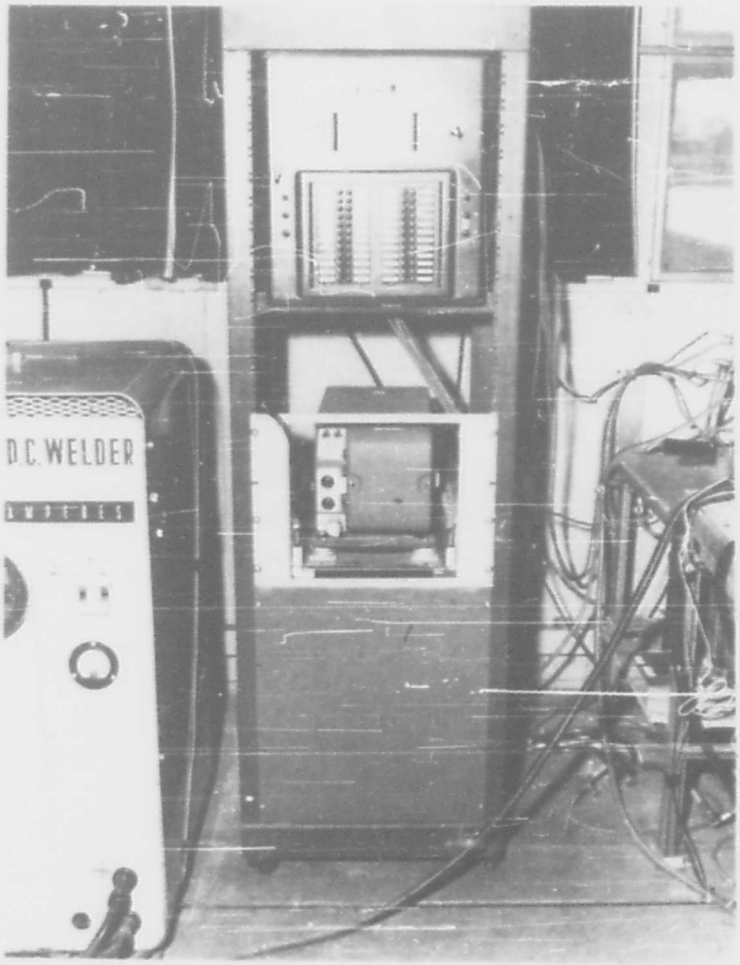

FIGURE 14

THERMOCOUPLE PYROMETER

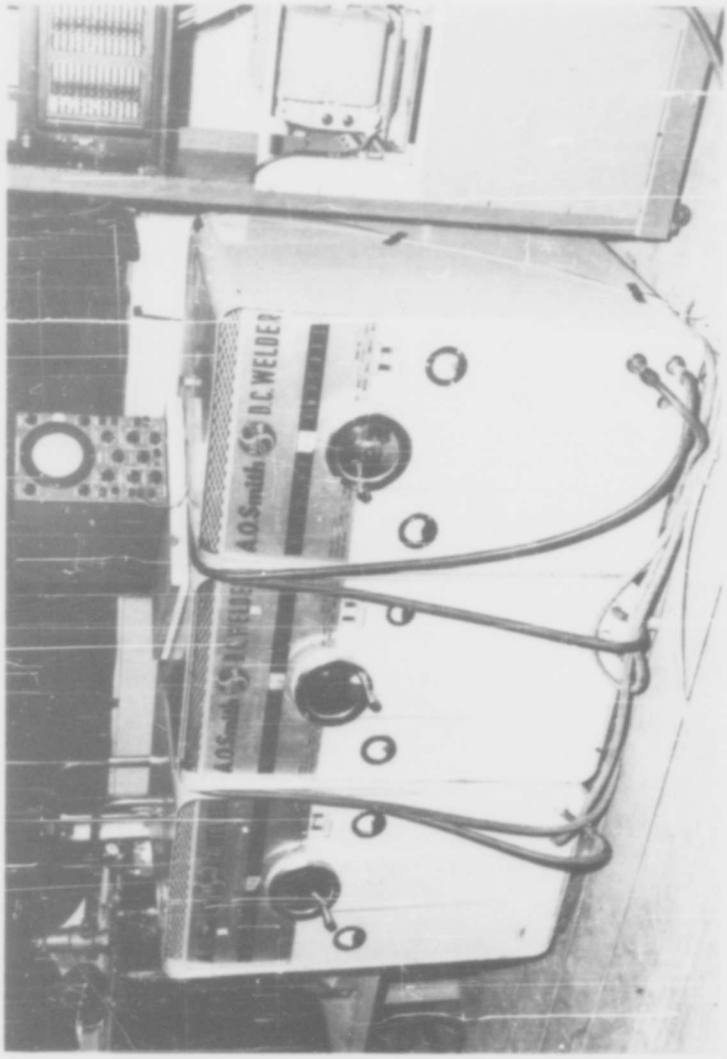

FIGURE 15

ARC POWER SUPPLY

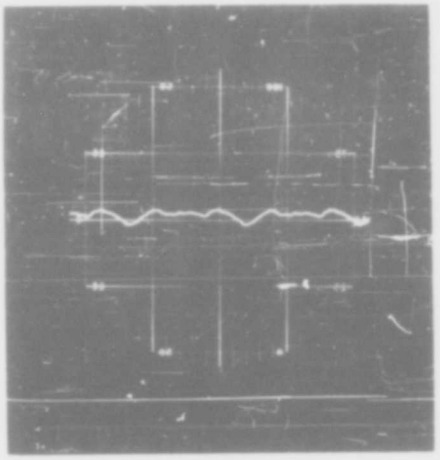

NO LOAD: I=0, V_t=55 volts

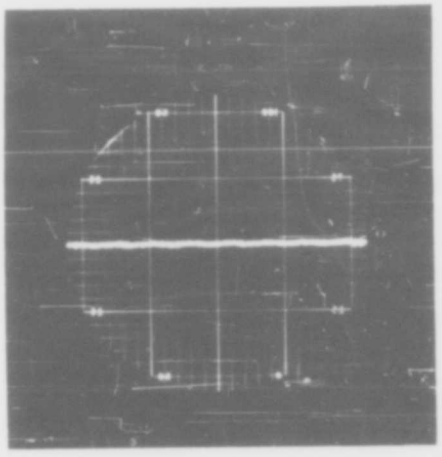

ARC-ON: I=40 amps, V_t=54 volts
(TWO-CHAMBER, Q=0.520 lb/sec-ft²)

FIGURE 16

POWER SUPPLY VOLTAGE RIPPLE
(VERTICAL SCALE: 10 v/SQUARE)

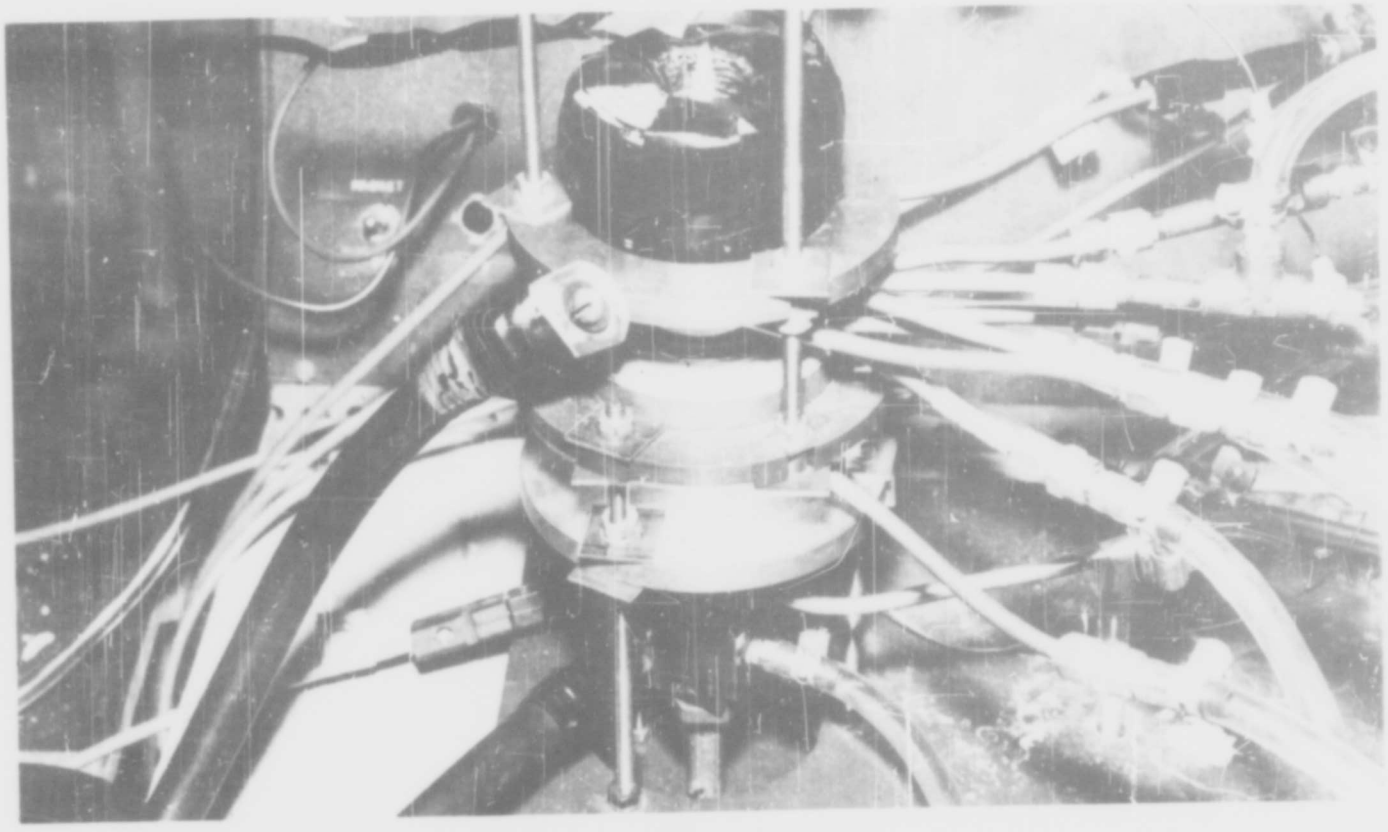

FIGURE 17

TWO-CHAMBER CONFIGURATION IN OPERATION

GA/MS/62-6

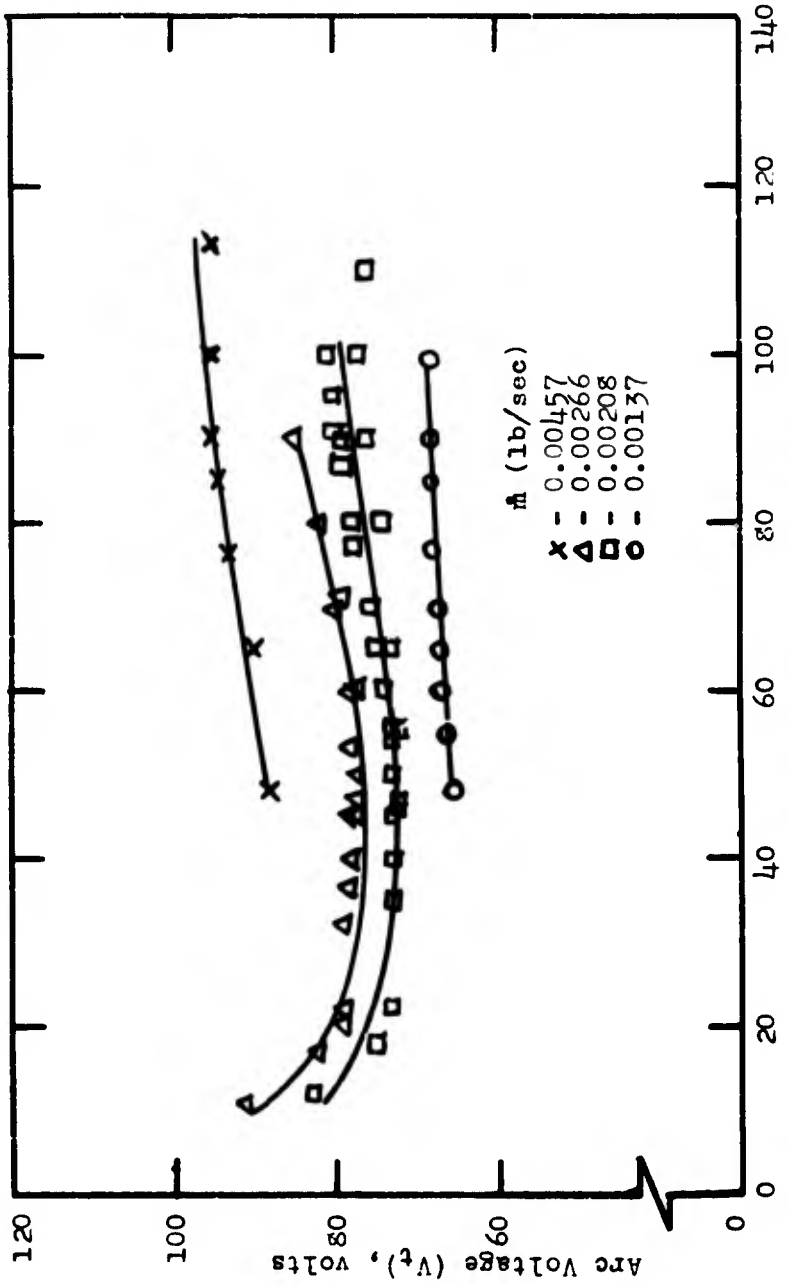

FIGURE 18

VOLT-AMPERE CHARACTERISTICS, CONFIGURATION A

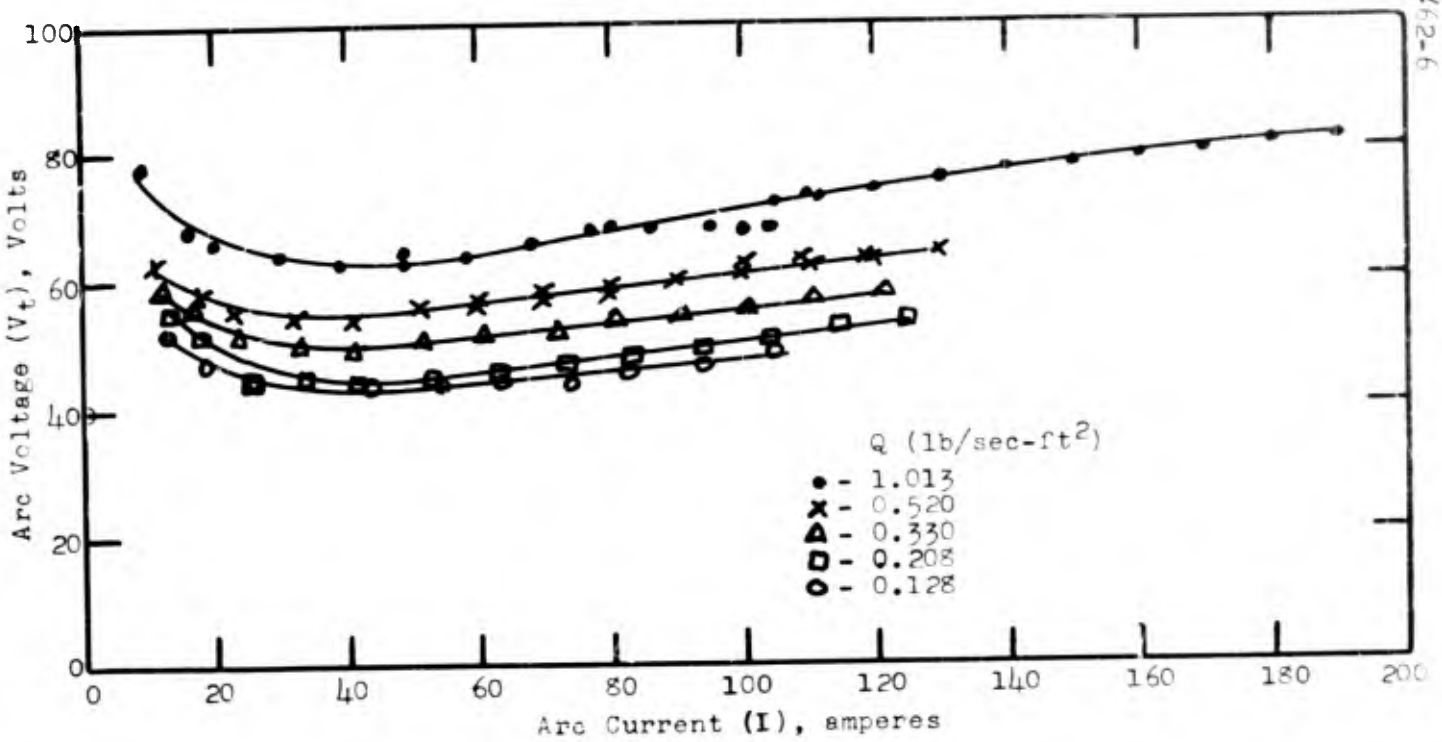

FIGURE 19

VOLT-AMPERE CHARACTERISTICS, CONFIGURATION B

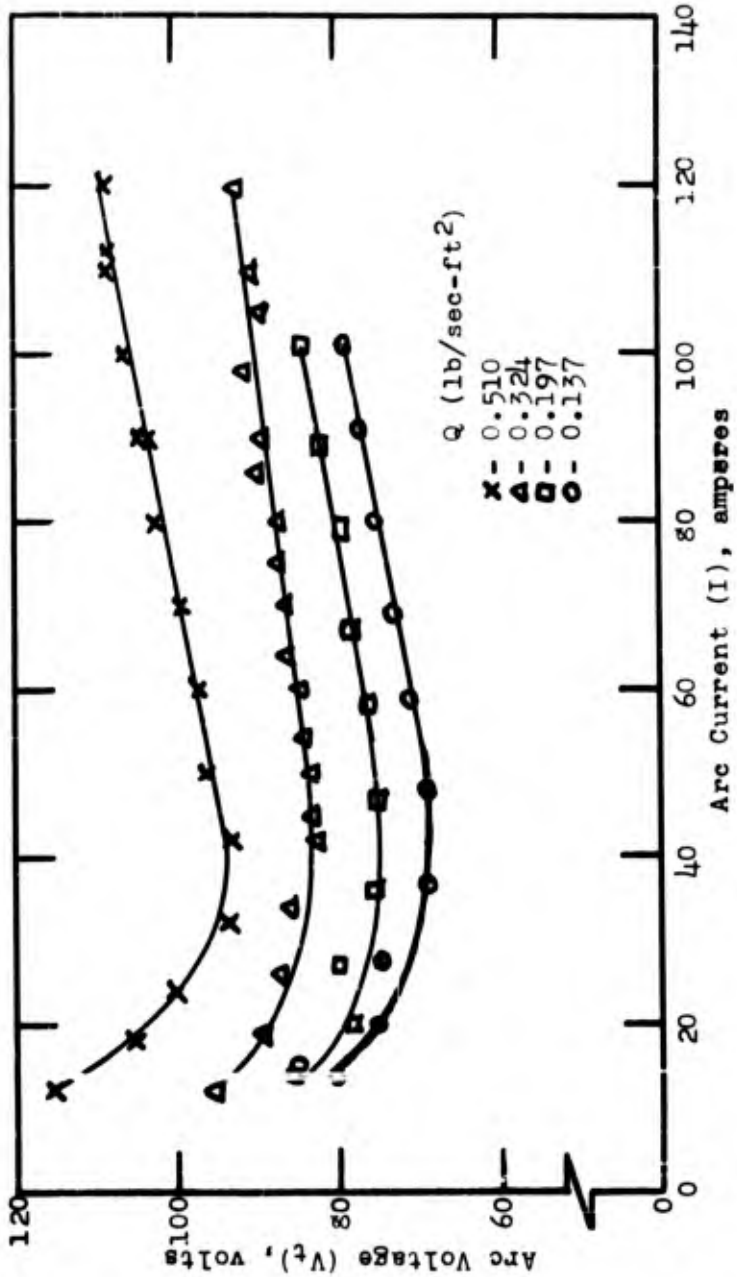

FIGURE 20

VOLT-AMPERE CHARACTERISTICS, CONFIGURATION C

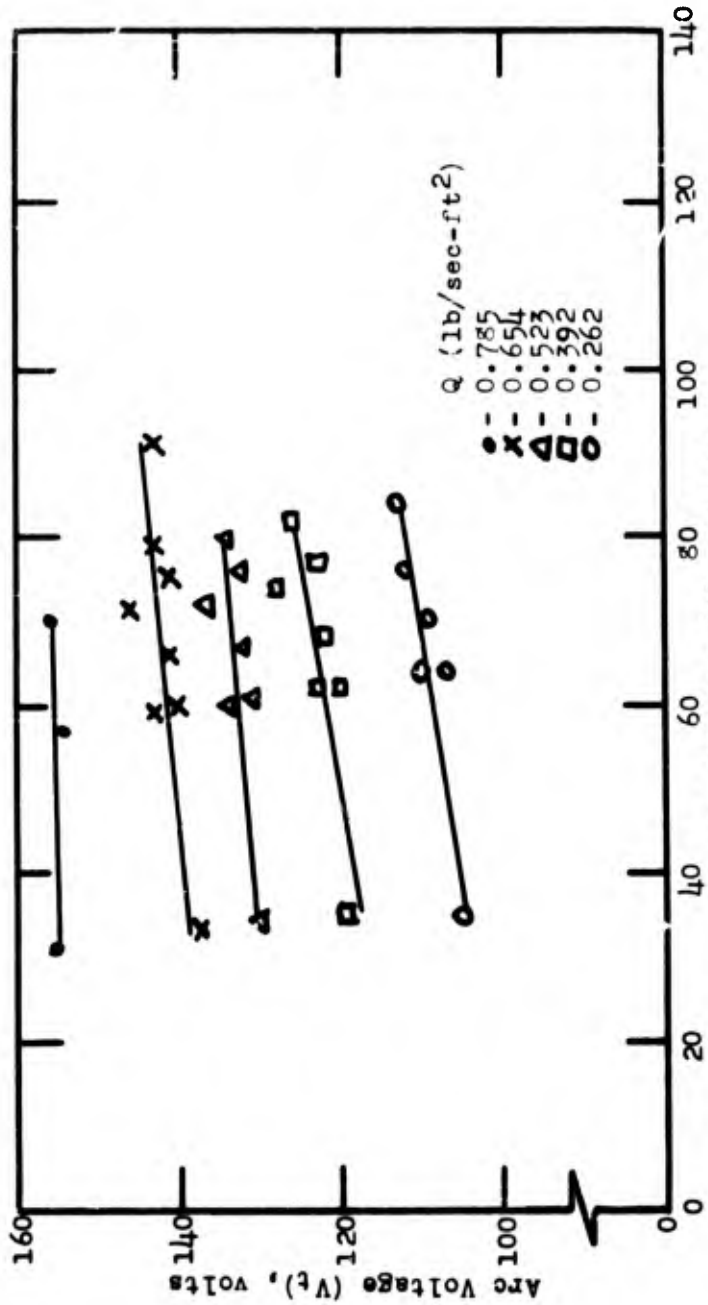

FIGURE 21

VOLT-AMPERE CHARACTERISTICS, CONFIGURATION D

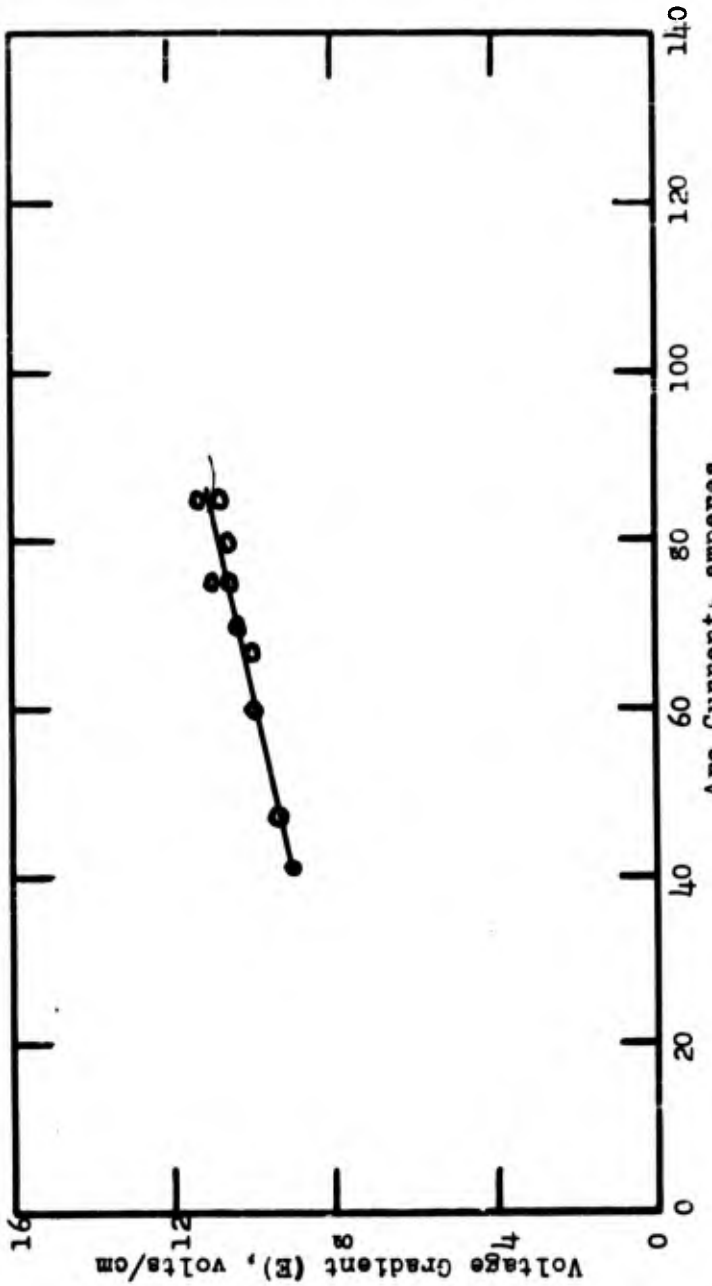

FIGURE 22

ARC COLUMN VOLTAGE GRADIENT, CONFIGURATION A, $\dot{m}$ = 0.00266 lb/sec

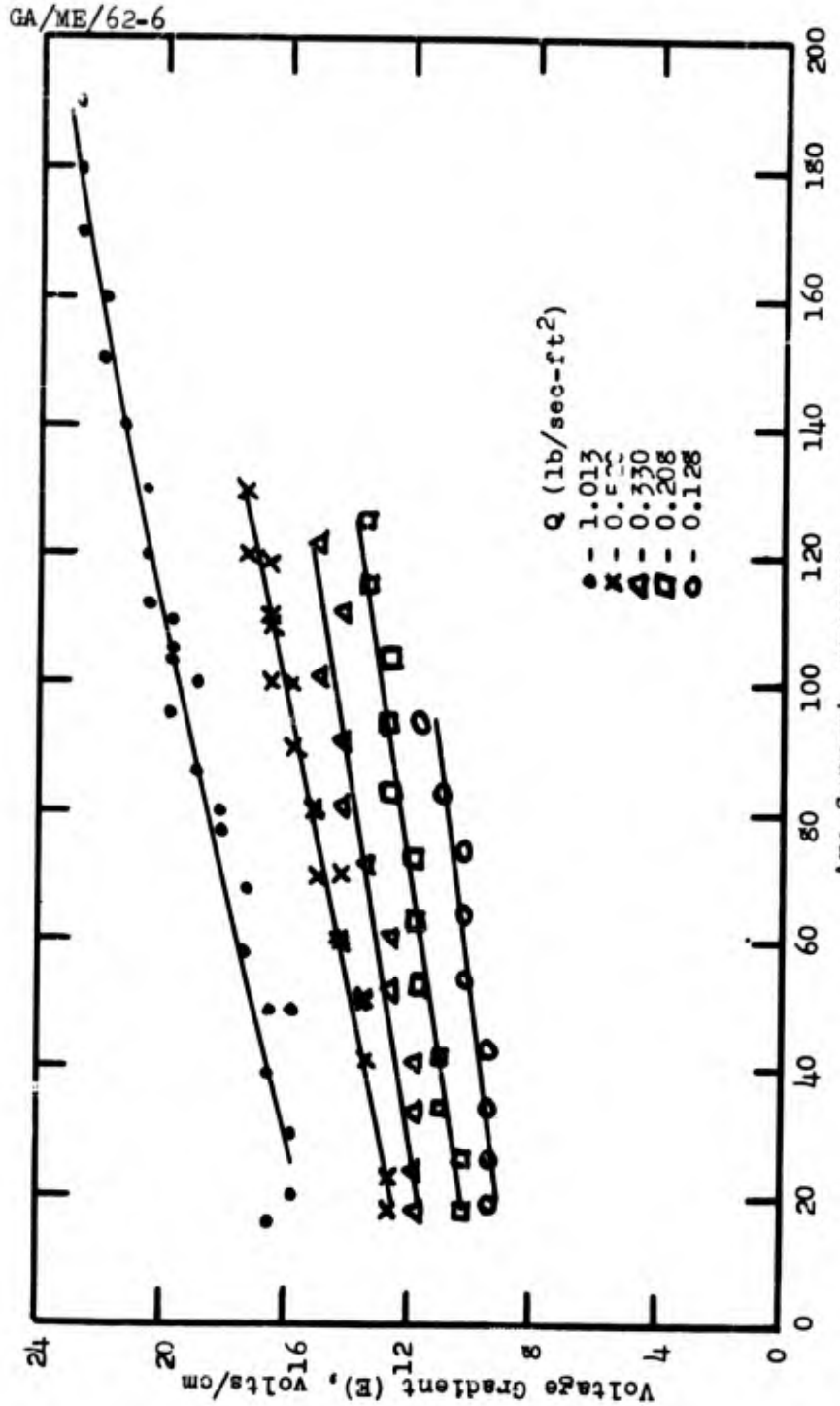

FIGURE 23

ARC COLUMN VOLTAGE GRADIENT, CONFIGURATION B

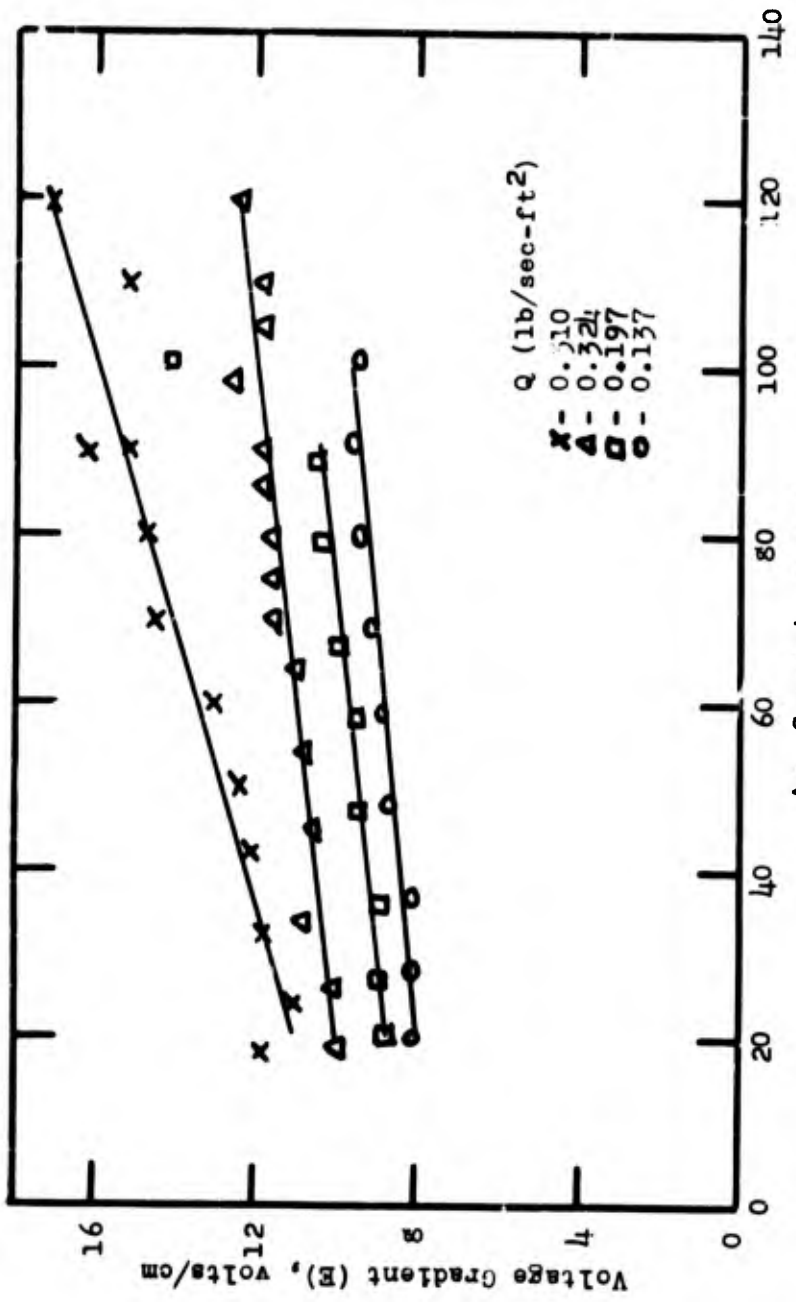

FIGURE 24

ARC COLUMN VOLTAGE GRADIENT, CONFIGURATION C

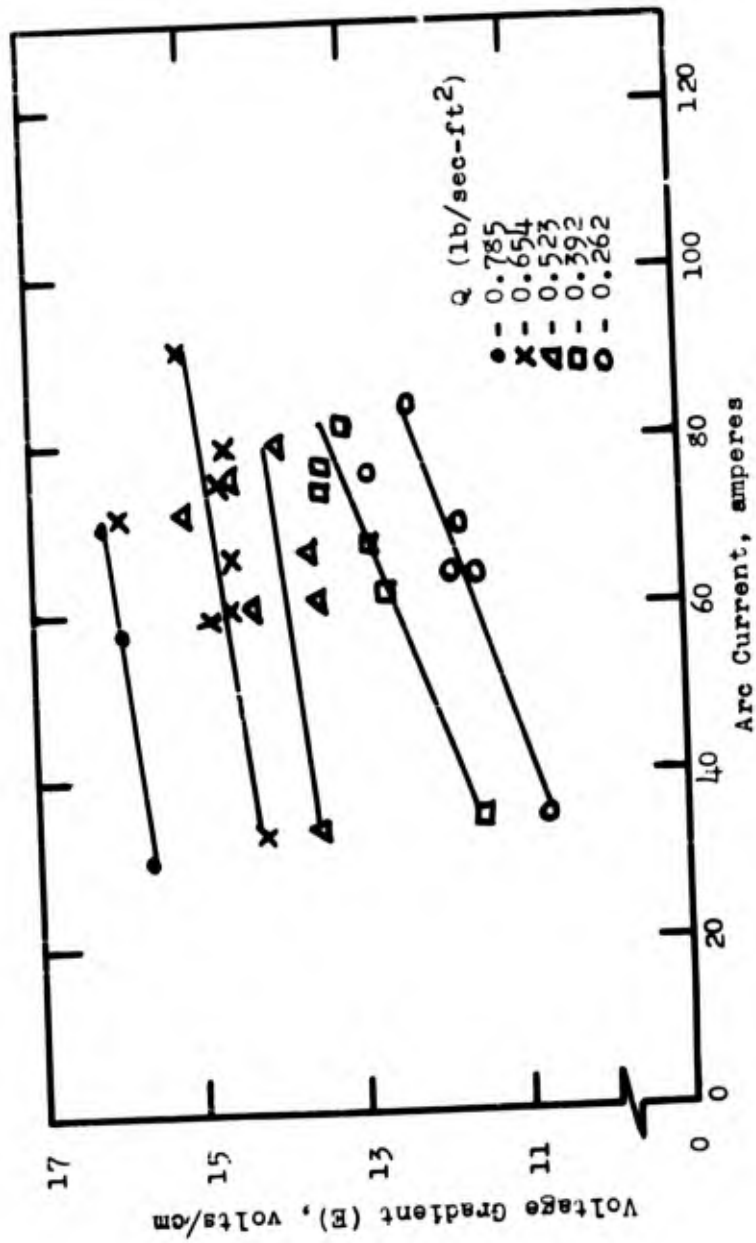

FIGURE 25

ARC COLUMN VOLTAGE GRADIENT, CONFIGURATION D

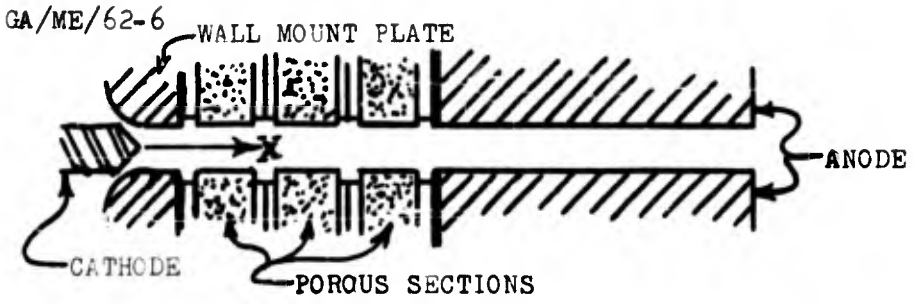

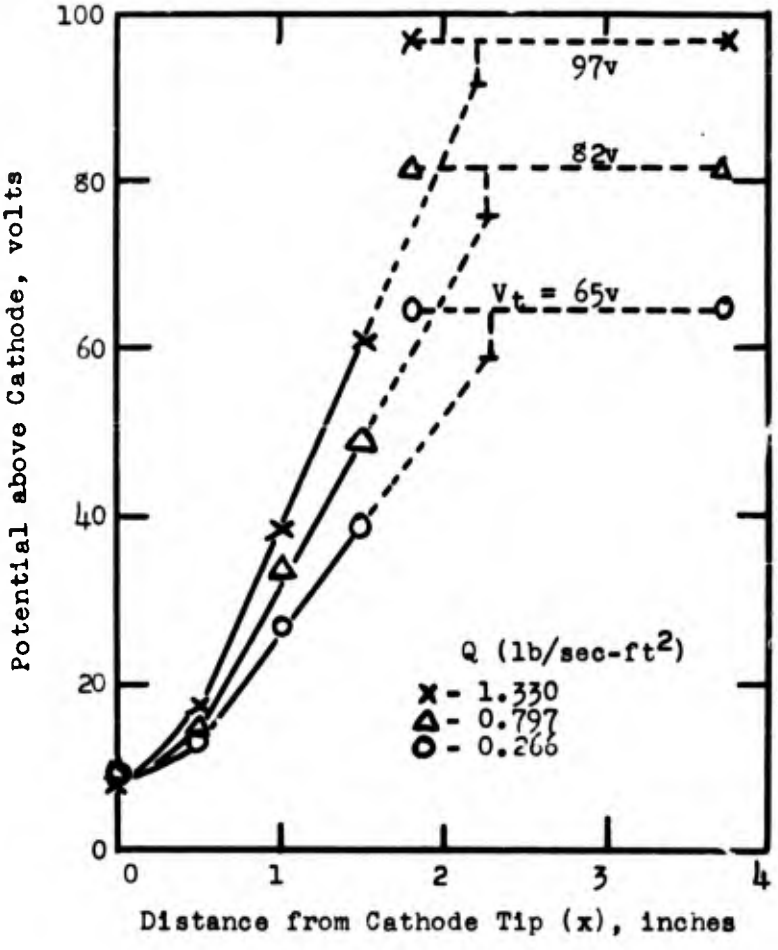

FIGURE 26

VOLTAGE DISTRIBUTION, CONFIGURATION E

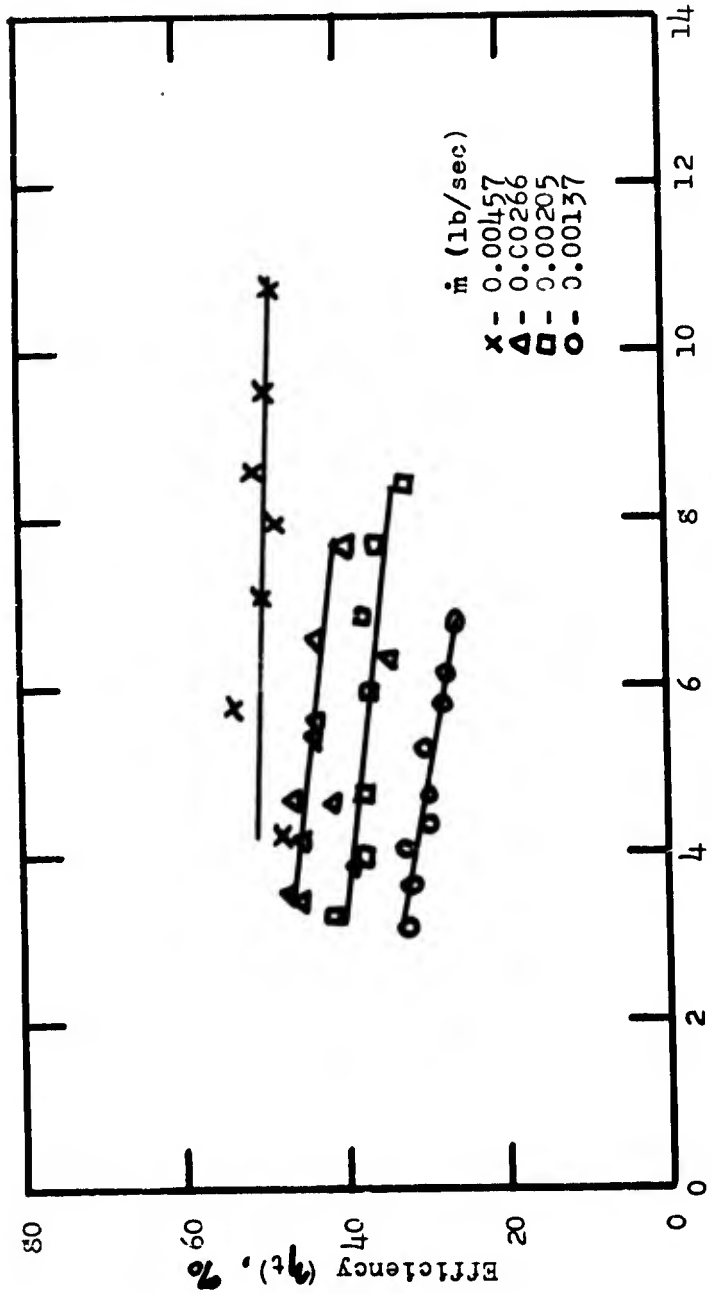

FIGURE 27

DEVICE EFFICIENCY, CONFIGURATION A

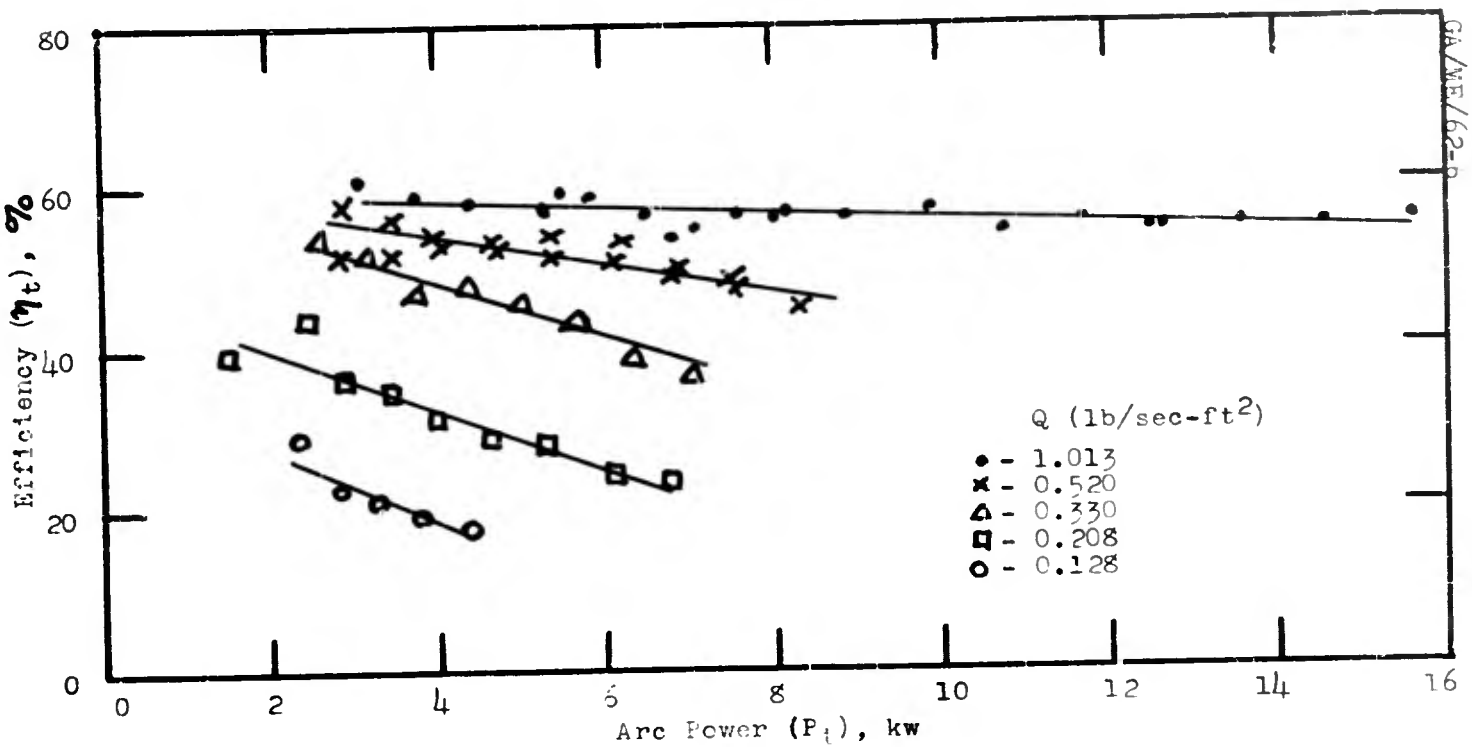

FIGURE 28

DEVICE EFFICIENCY, CONFIGURATION B

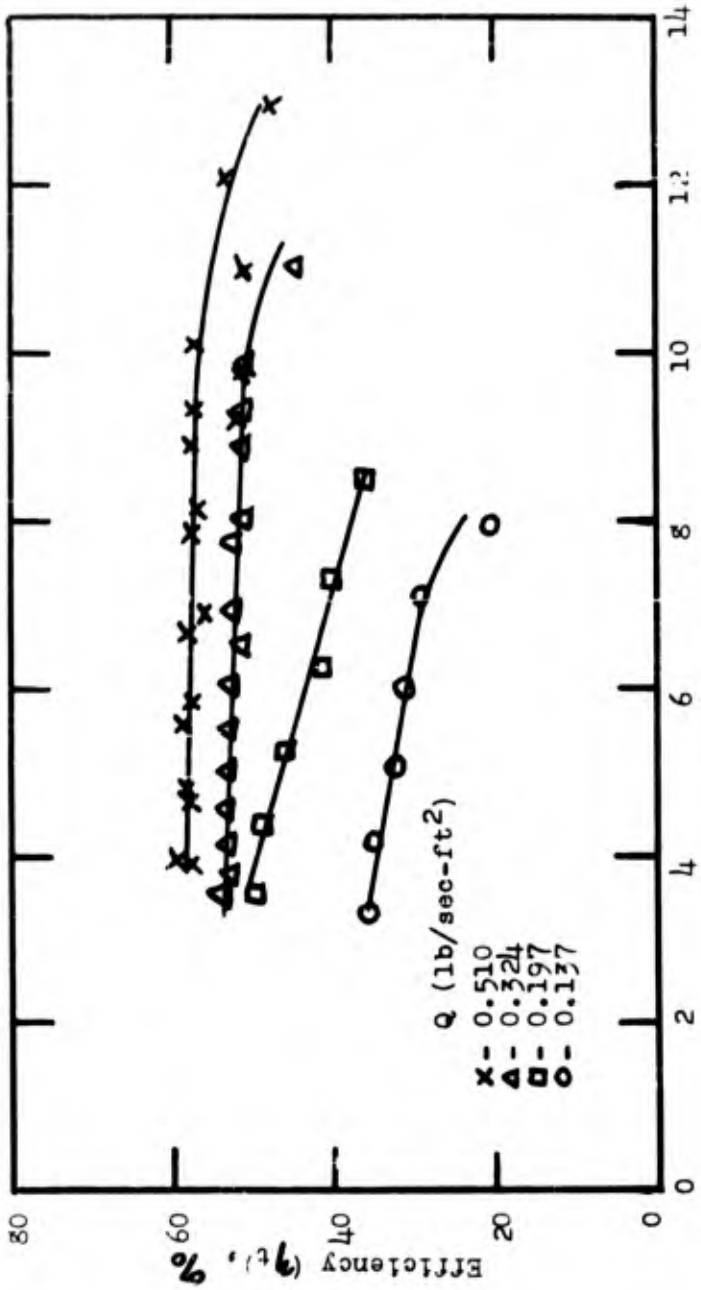

FIGURE 29

DEVICE EFFICIENCY, CONFIGURATION C

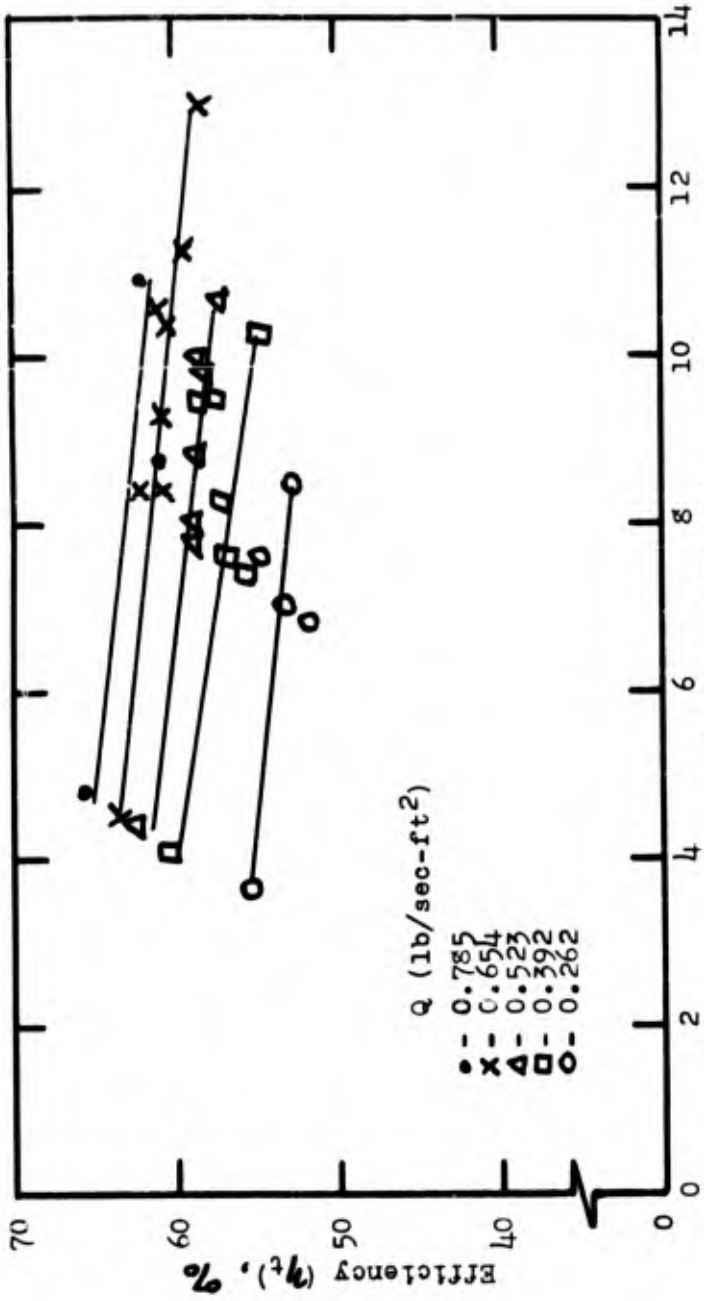

FIGURE 30

DEVICE EFFICIENCY, CONFIGURATION D

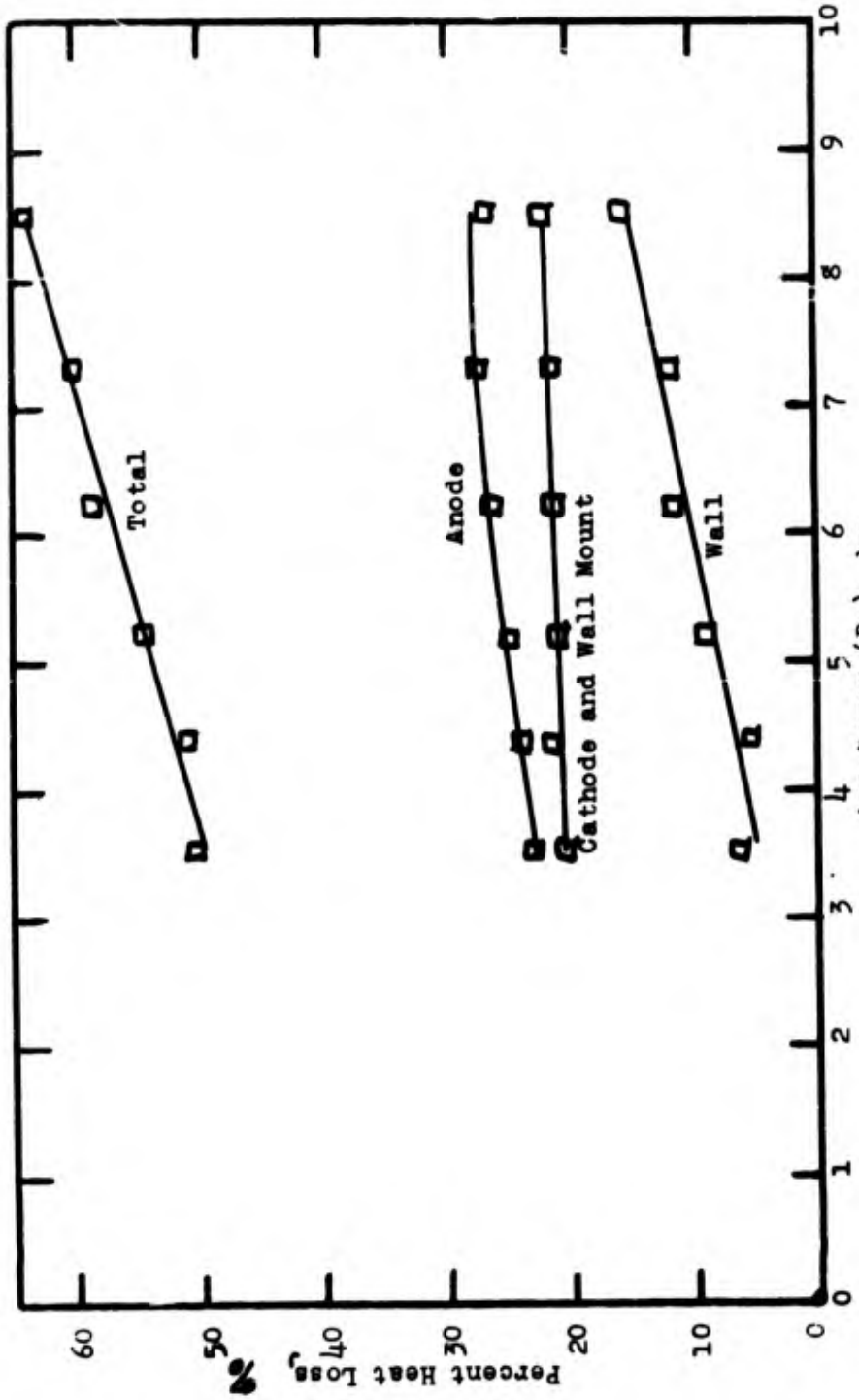

FIGURE 31

COMPONENT HEAT LOSS, CONFIGURATION C, Q = 0.197 lb/sec-ft2

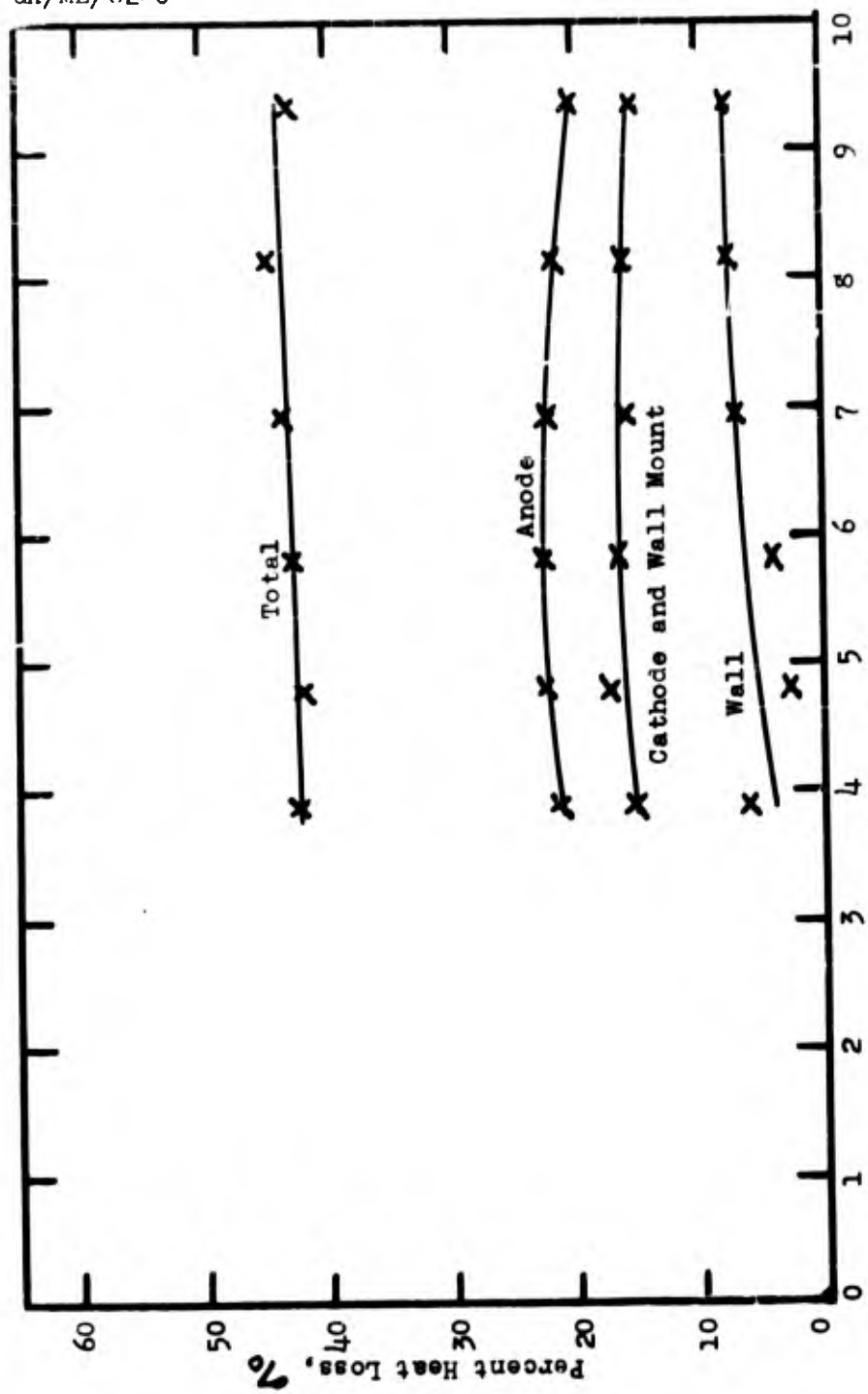

FIGURE 32

COMPONENT HEAT LOSS, CONFIGURATION C, Q = 0.510 lb/sec-ft^2

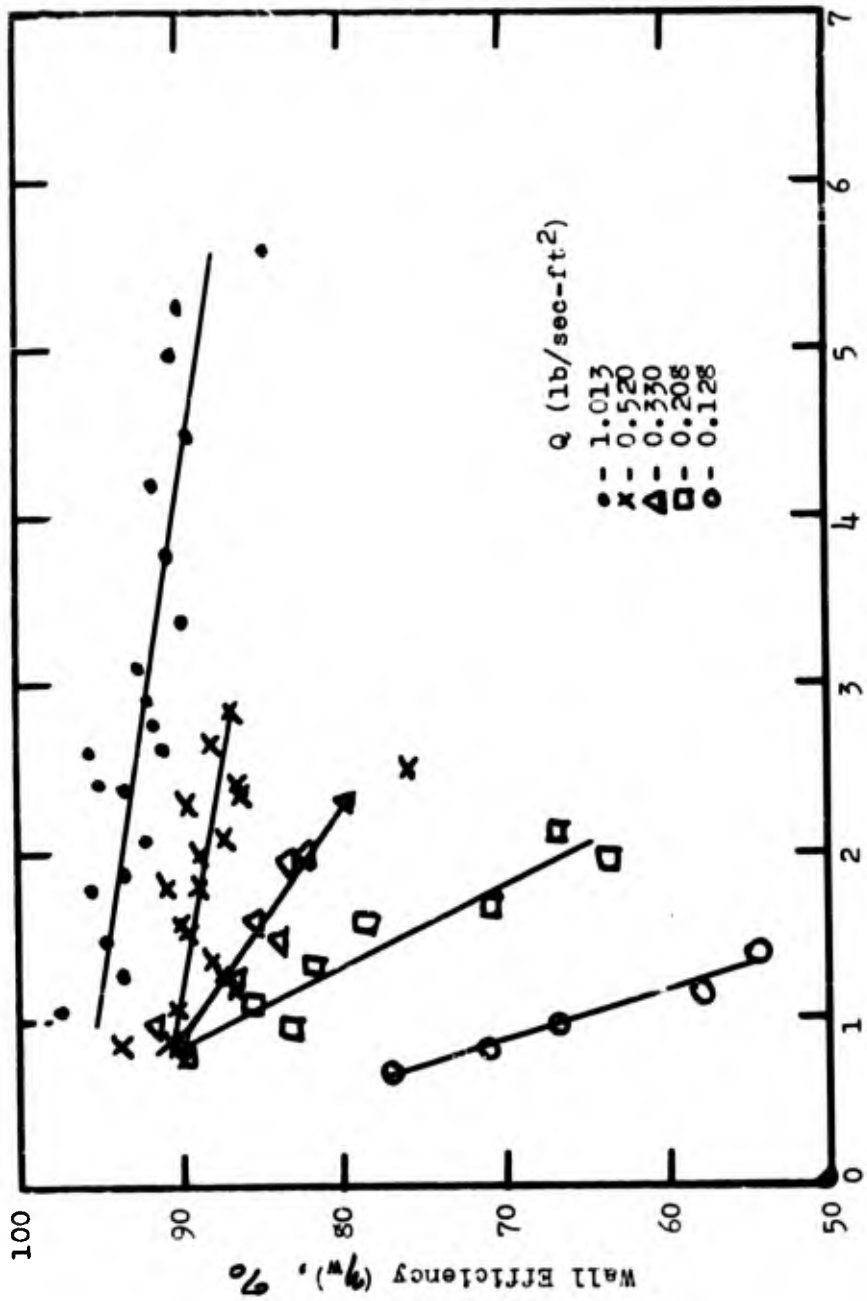

FIGURE 33

WALL EFFICIENCY, CONFIGURATION B

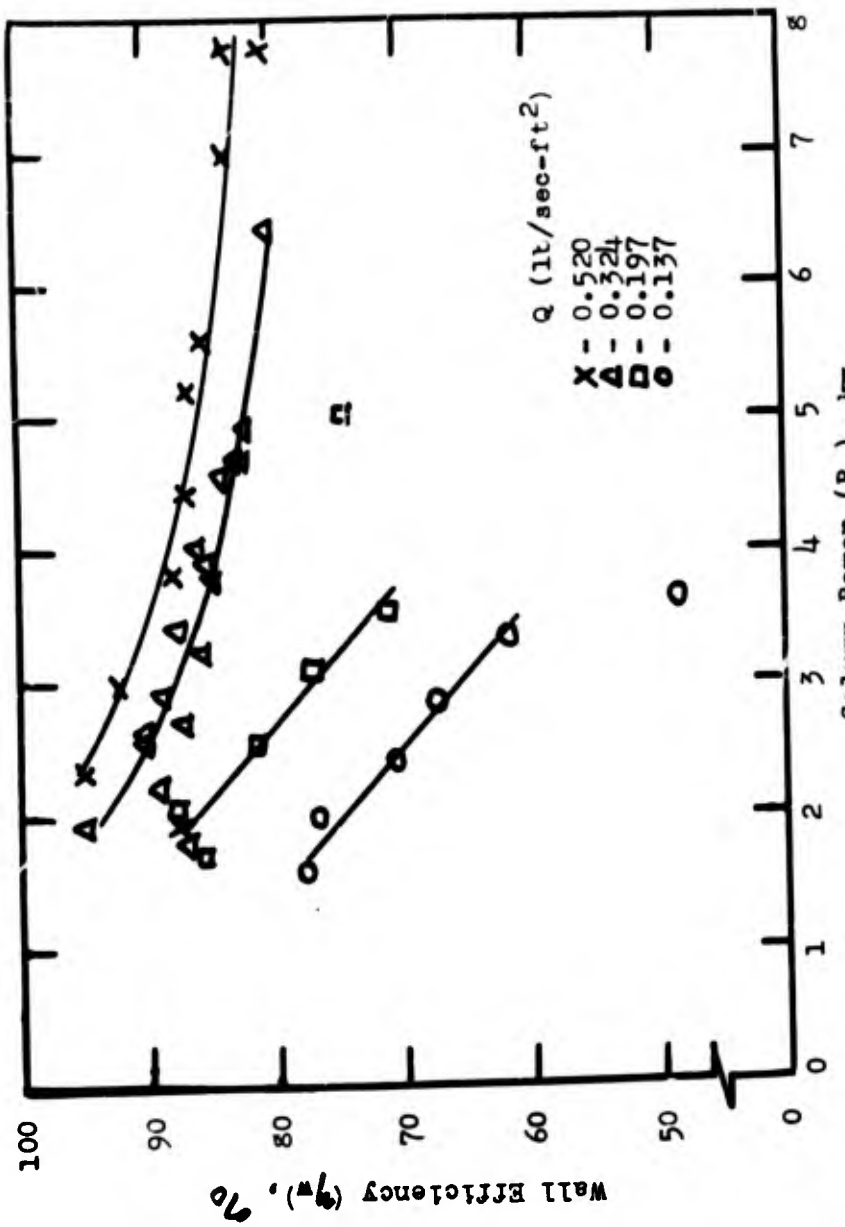

FIGURE 34

WALL EFFICIENCY, CONFIGURATION C

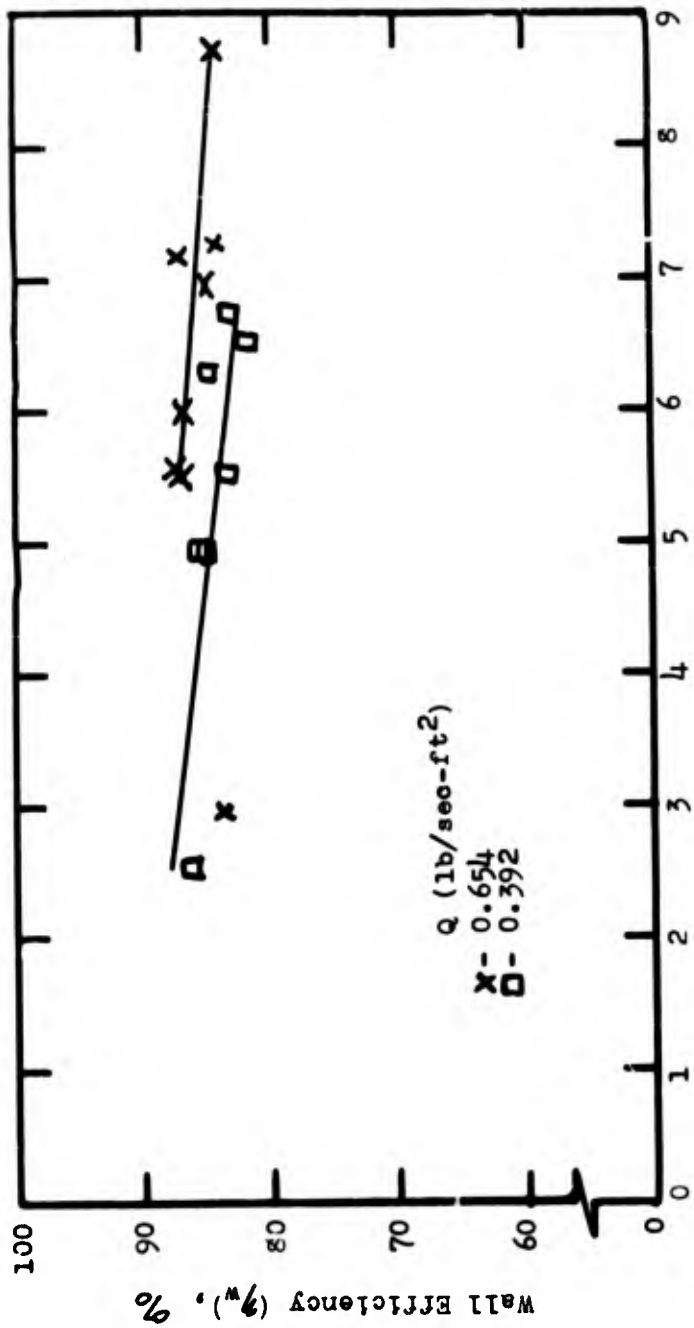

FIGURE 35

WALL EFFICIENCY, CONFIGURATION D

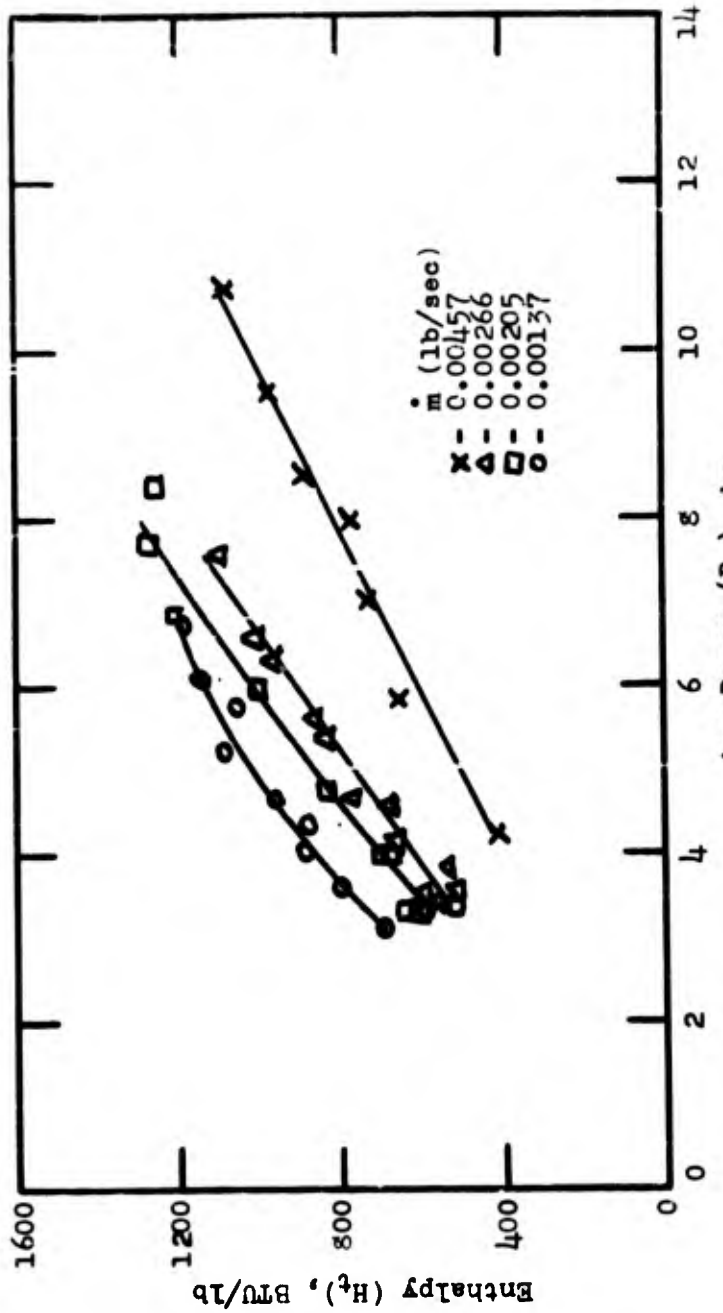

FIGURE 36

GAS ENTFALPY RISE, CONFIGURATION A

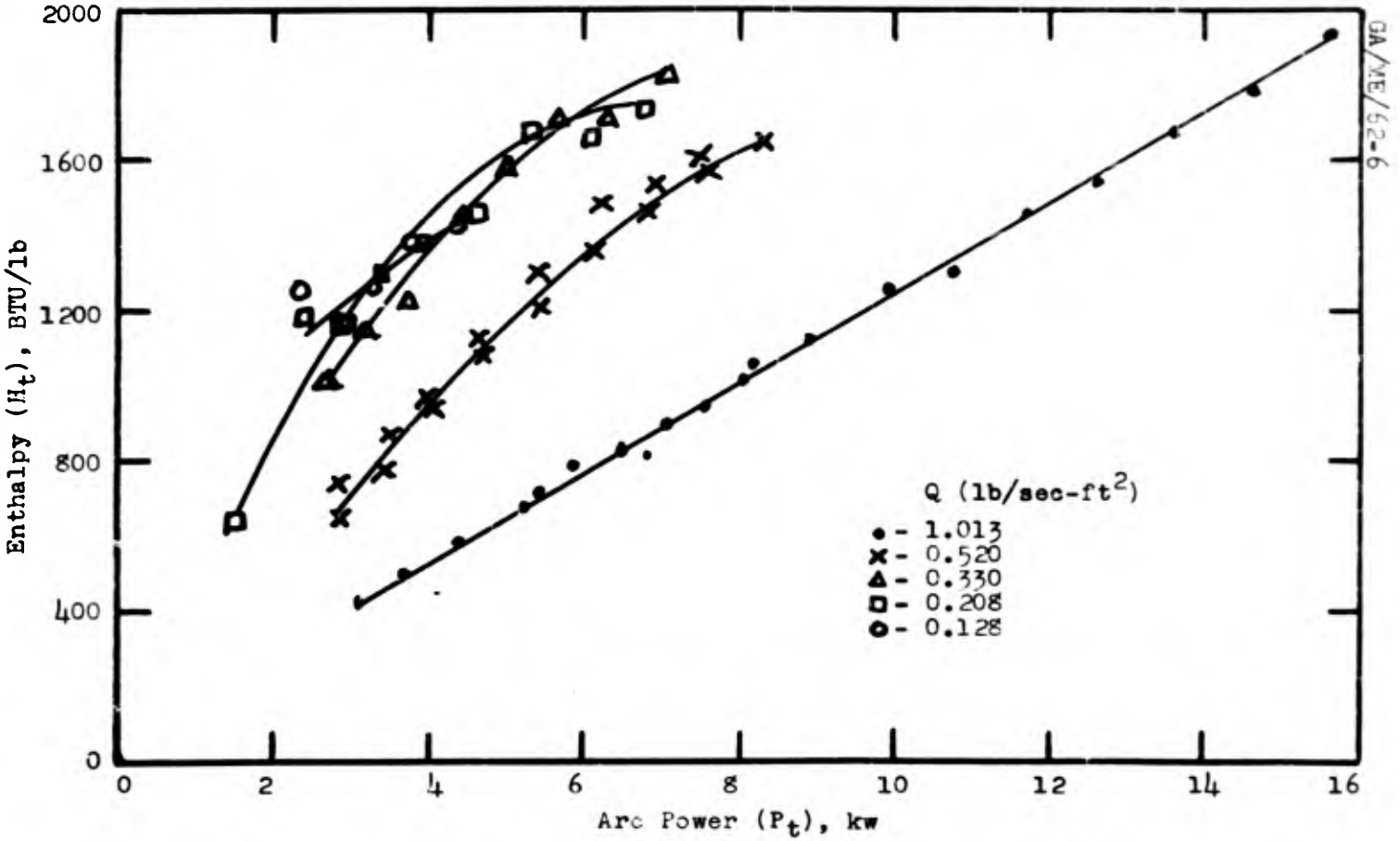

FIGURE 37

GAS ENTHALPY RISE, CONFIGURATION B

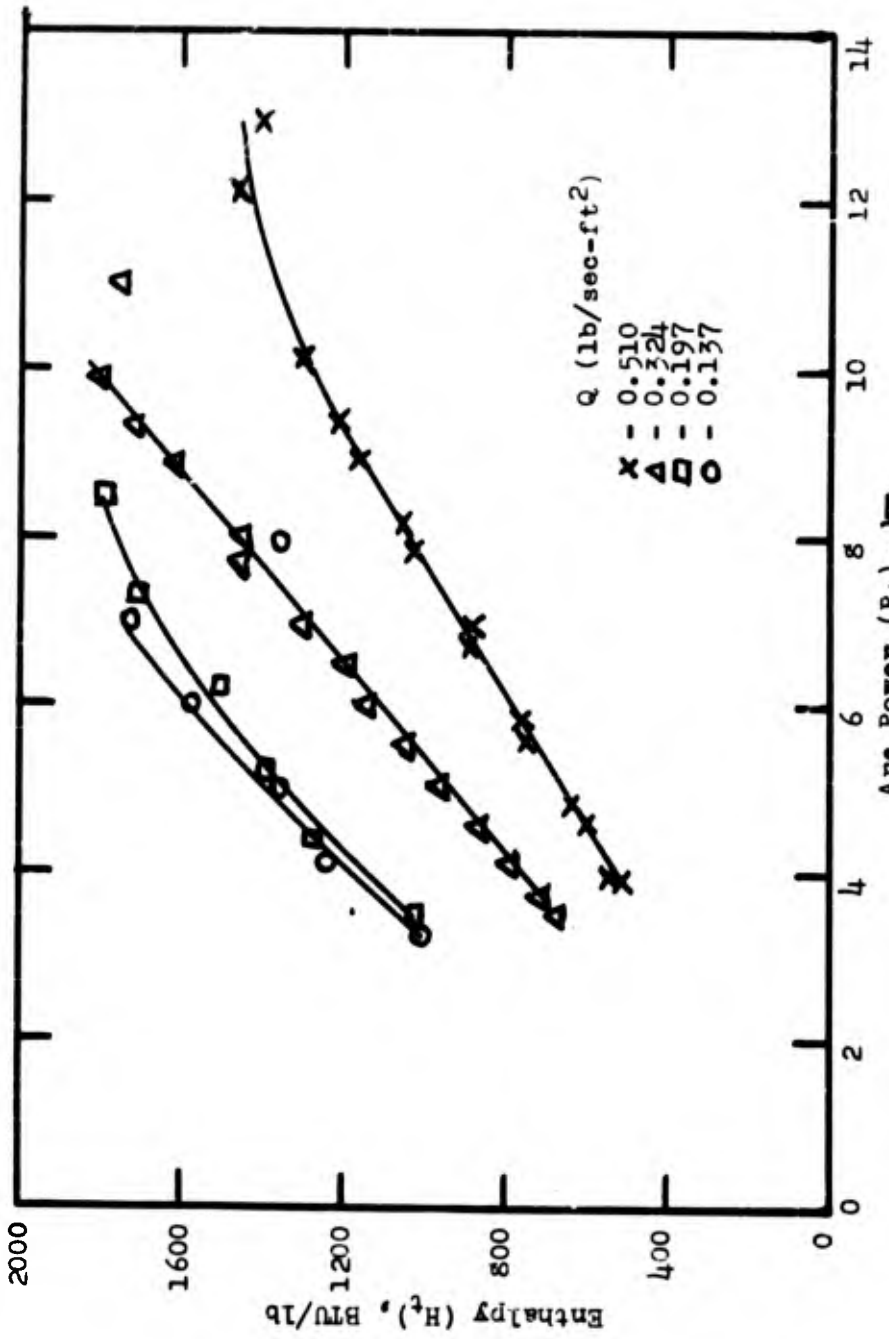

FIGURE 38

GAS ENTHALPY RISE, CONFIGURATION C

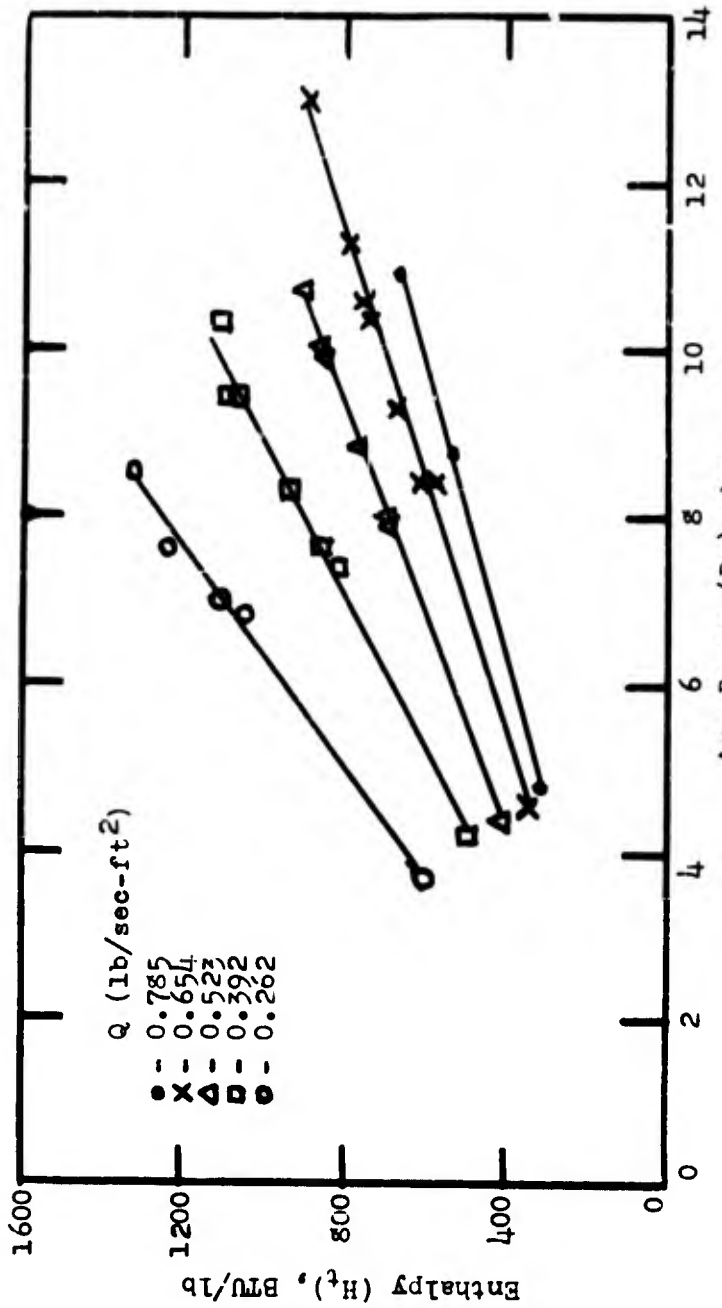

FIGURE 39

GAS ENTHALPY RISE, CONFIGURATION D

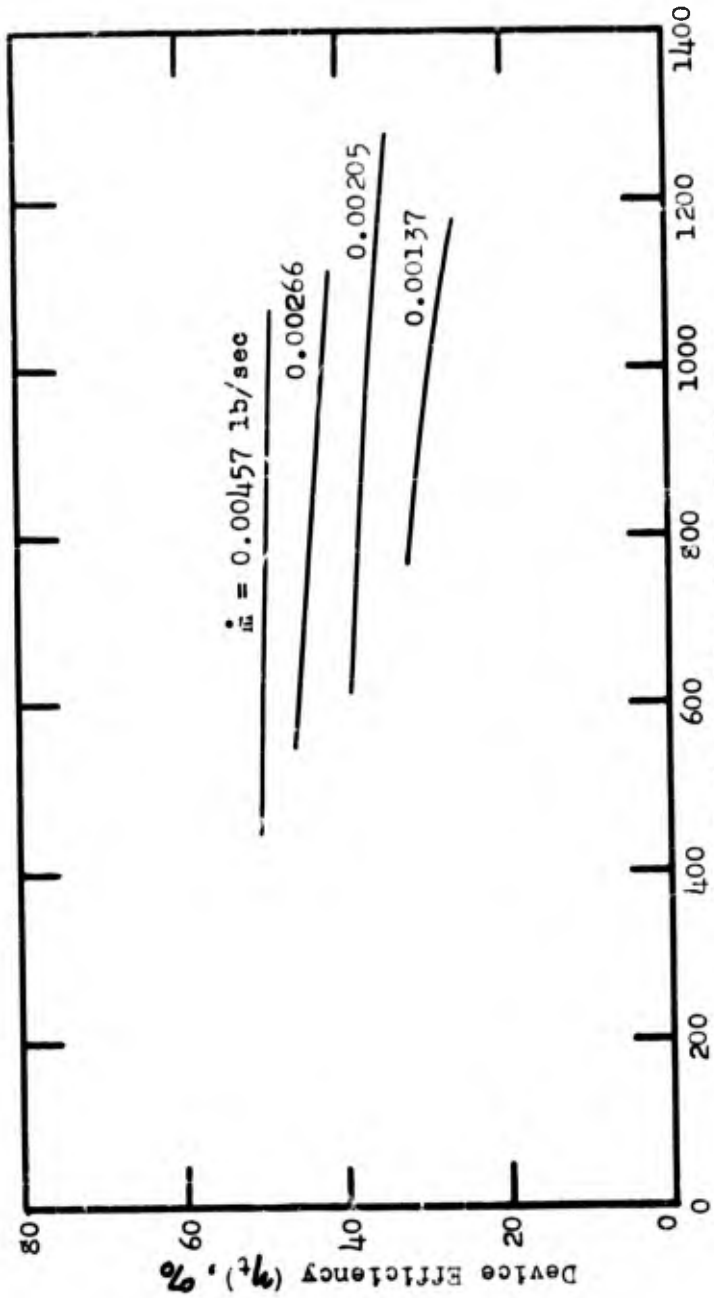

FIGURE 40

DEVICE PERFORMANCE, CONFIGURATION A

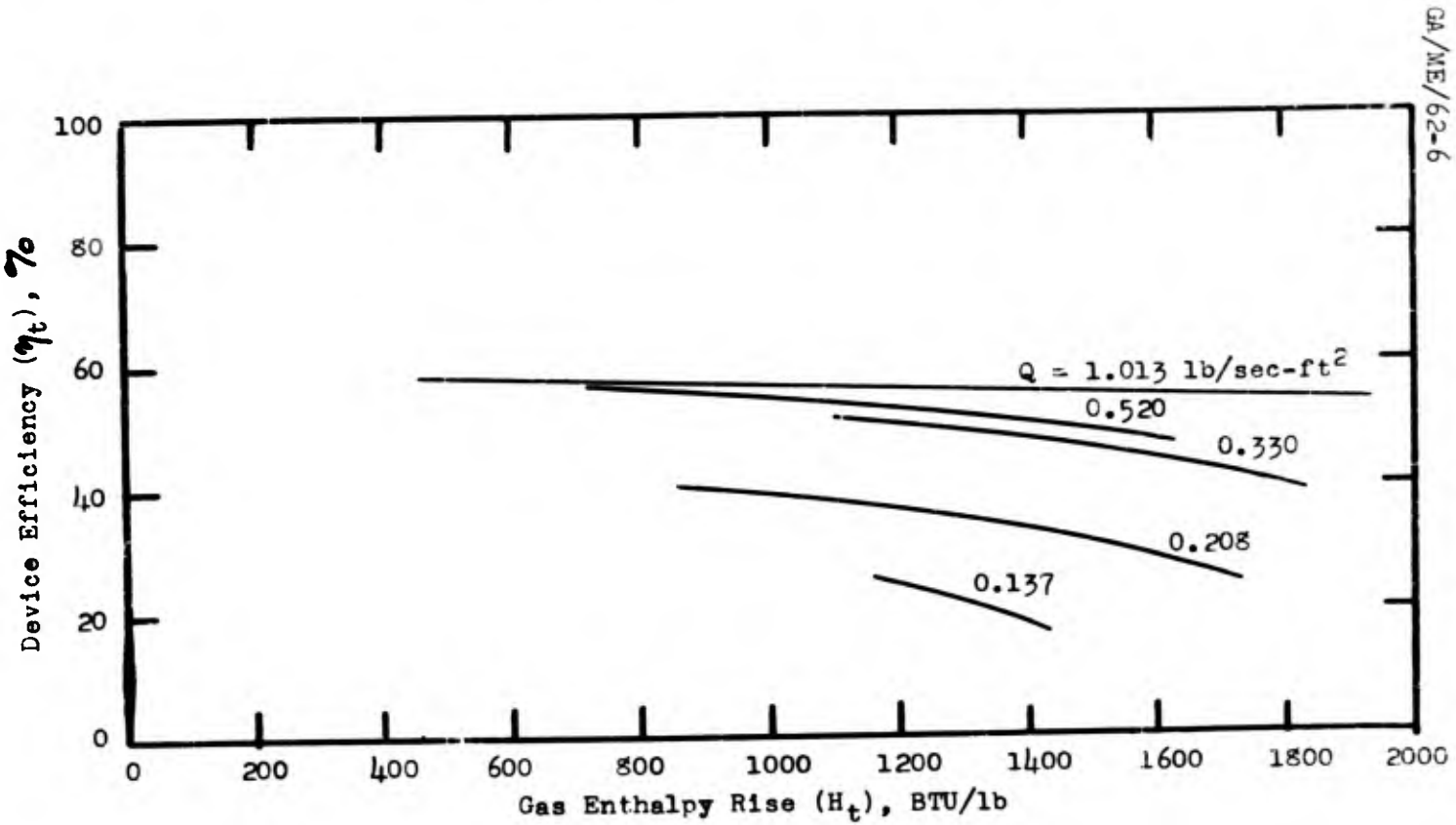

FIGURE 41

DEVICE PERFORMANCE, CONFIGURATION B

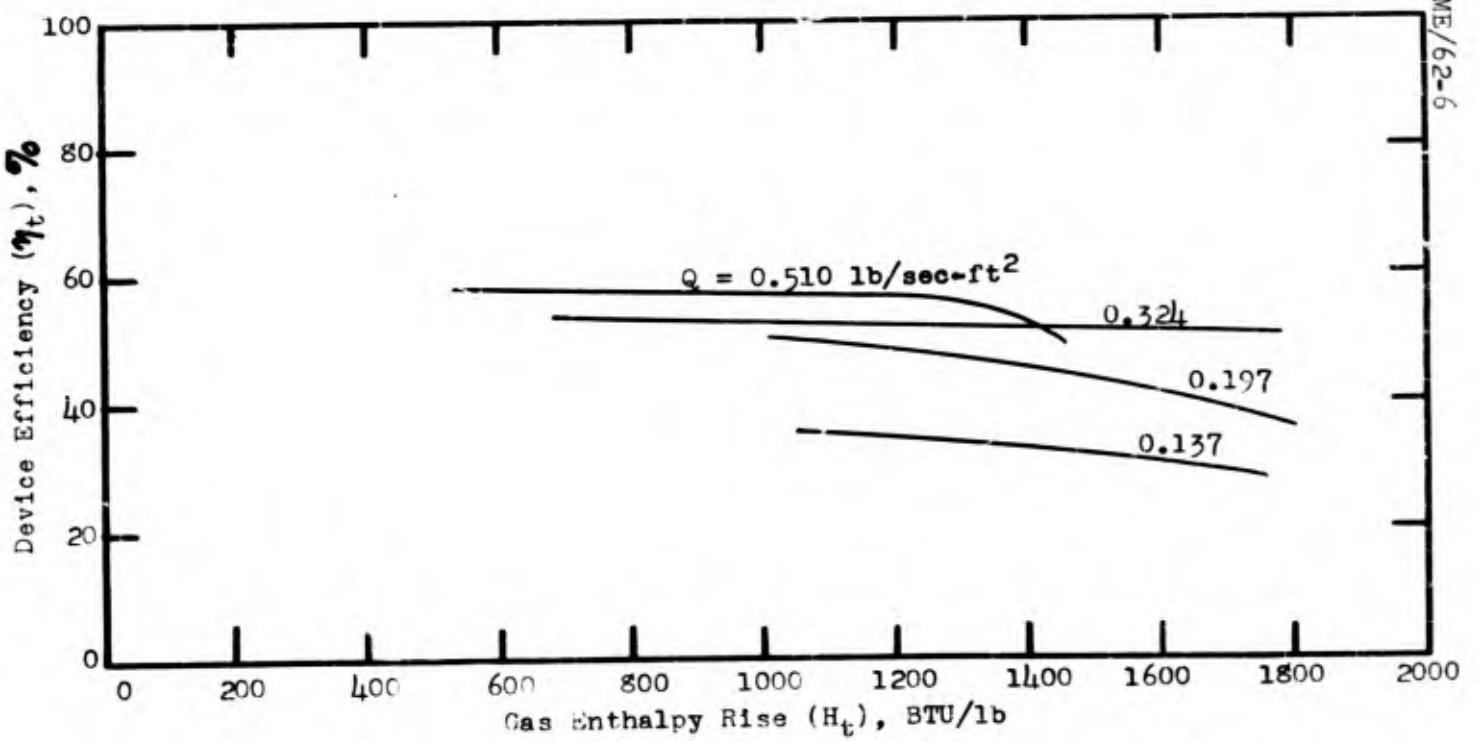

FIGURE 42

DEVICE PERFORMANCE, CONFIGURATION C

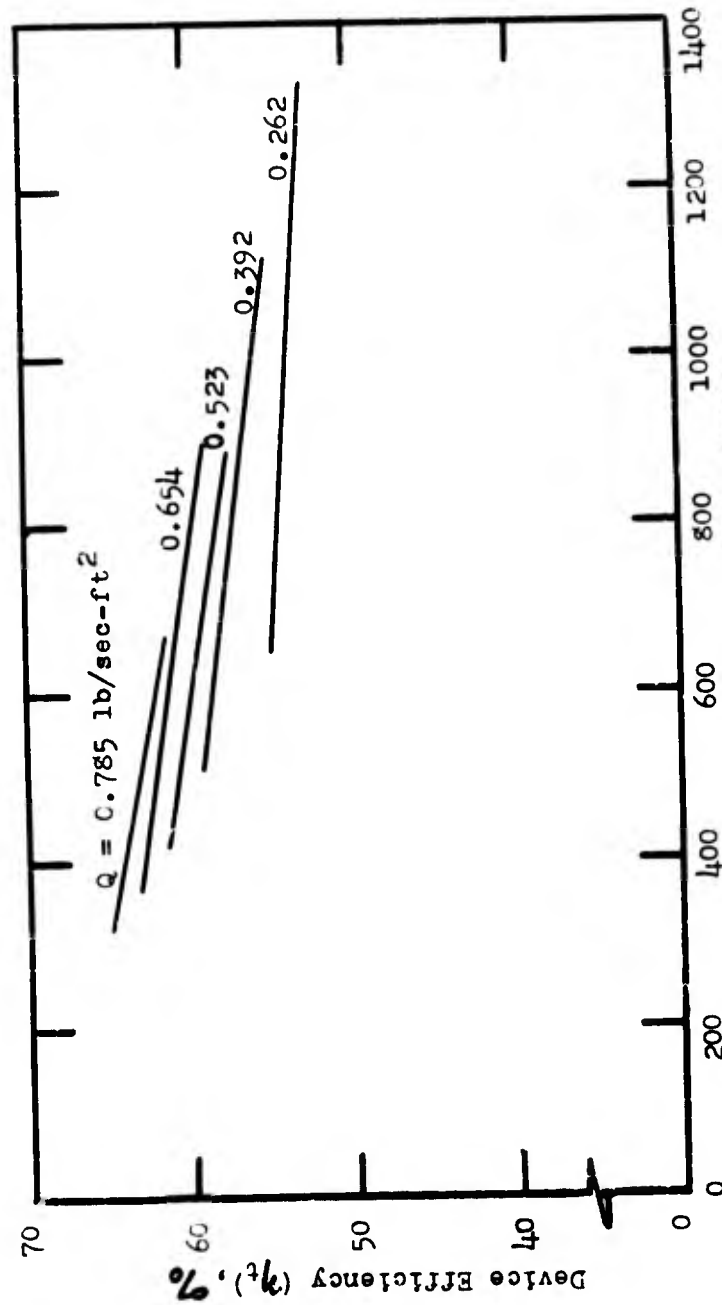

FIGURE 43

DEVICE PERFORMANCE, CONFIGURATION D

TABLE I

RANGE OF GAS FLOWS

CONFIGURATION	TOTAL MASS FLOW $\dot{m}$ lb/sec	TRANSPIRATION RATE Q lb/sec-ft^2	LONGITUDINAL MASS VELOCITY W lb/sec-ft^2
A	1.37×10^{-3} 2.05 2.66 4.57	--- --- --- ---	4.02 6.01 7.81 13.40
B	0.259×10^{-3} 0.523 0.854 1.110 1.36 1.61 2.12 2.62 3.14 4.15	0.061 0.128 0.208 0.271 0.330 0.393 0.520 0.640 0.767 1.013	0.76 1.54 2.51 3.26 3.98 4.72 6.22 7.72 9.22 12.20
C	0.528×10^{-3} 1.12 1.62 2.14 2.66 3.18 4.17	0.064 0.137 0.197 0.261 0.324 0.387 0.510	1.55 3.29 4.75 6.25 7.77 9.34 12.30
D	3.213×10^{-3} 4.82 6.43 8.03 9.64	0.262 0.392 0.523 0.654 0.785	9.44 14.2 18.8 23.6 28.3

TABLE II

SAMPLE OF RAW DATA, CONFIGURATION B

GAS FLOW ft^3/hr	I amps	V_t volts	V_w volts	T_c ^oF	T_w ^oF	T_{in} ^oF	T_{out} ^oF	T_{w1} ^oF	T_{w2} ^oF	WATER lb/sec
50	0	0	0	86	64	65	65	63	63	0.0764
	12	59	--	--	--	--	--	--	--	--
	18	56	15	--	--	--	--	--	--	--
	24	51	15	--	--	--	--	--	--	--
	33	50	15	--	--	--	--	--	--	--
	41	49	15	--	--	--	--	--	--	--
	52	51	16	87	98	67	82	72	73	.0764
	61	52	16	87	110	67	86	74	75	.0764
	72	52	17	87	125	67	92	75	77	.0764
	81	54	18	87	132	67	96	77	80	.0764
	91	55	18	87	150	67	101	79	82	.0764
	101	56	19	87	160	67	107	81	85	.0764
	111	57	18	87	185	67	100	78	81	0.1120
	122	58	19	87	220	67	105	79	83	0.1120

TABLE III

CONDUCTIVITY EXPERIMENT, CONFIGURATION F

Q lb/sec-ft^2	I amps	E v/cm	d cm	ESTIMATED			LOWER BOUND		
				j amps/cm^2	σ mho/cm	T ^oK	j amps/cm^2	σ mho/cm	T ^oK
0.398	43	11.8	0.309	573	48.6	12,500	136	11.5	8,000
0.796	40	15.6	0.253	798	50.9	13,000	126	6.0	7,500

TABLE IV

HEAT TRANSFER COMPARISON, CONFIGURATION E

Case	$\dot{m}$ lb/sec	$\dot{m}/A$ lb/sec-ft^2	P_{Lw}/A_w BTU/sec-ft^2	T_c ^oR	T_w ^oR	T_B ^oR	$Qc_p(T_w-T_c)$ BTU/sec-ft^2	h BTU/hr-ft^2-^oR
Axial Flow	0.00137	---	18.2	540	795	5000	---	15.7
	.00266	---	27.2	540	790	3200	---	39.5
	.00383	---	27.2	540	780	2200	---	65.7
Transpiration Cooled	0.00137	0.223	3.18	540	568	5400	0.714	3.0
	.00266	.433	3.18	540	551	3900	.590	4.1
	.00383	.623	1.58	540	547	2900	.540	3.3

APPENDIX A

Sample Computations

Appendix A

Sample Computations

The data used in the following computations are from Table II.

Gas Flow Quantities

Gas Flow = 50 ft^3/hr

$$\dot{m} = \frac{\text{Gas Flow}}{3600 \text{ sec/hr}} \times \text{density at room conditions}$$

density = 0.0974 lb/ft^3

$$\dot{m} = \frac{50 \times 0.0974}{3600} = \underline{1.35 \times 10^{-3} \text{ lb/sec}}$$

$$G = \frac{\dot{m}}{A_w} \qquad (A_w = \text{Wall Area})$$

$$A_w = \frac{\pi \times .25 \times .375}{144} \times \text{No. of chambers} = 2.05 \text{ N} \times 10^{-3} \text{ ft}^2$$

N = 2 for configuration B

$$\underline{G} = \frac{1.35 \times 10^{-3}}{4.1 \times 10^{-3}} = \underline{0.330 \text{ lb/sec-ft}^2}$$

$$W = \frac{\dot{m}}{A_c} \qquad (A_c = \text{Exit Area})$$

$$A_c = \frac{\pi (.25)^2}{4 \times 144} = 3.4 \times 10^{-4} \text{ ft}^2$$

$$W = \frac{1.35 \times 10^{-3}}{3.4 \times 10^{-4}} = 3.98 \text{ lb/sec-ft}^2$$

Power

$P_t = IV_t = 61 \times 52 = \underline{3.17 \text{ kw}}$

$P_c = IV_w = 61 \times 16 = \underline{0.976 \text{ kw}}$

$P_{Lt} = \dot{m}_w C_{pw} (Tout - Tin)$

$\dot{m}_w$ = water flow rate = 0.0764 lb/sec

C_{pw} = specific heat of water = 1.055 $\frac{\text{kw-sec}}{16-^\circ R}$

Tout = 86 Tin = 67

$P_{Lt} = 0.0764 \times 1.055 (19) = \underline{1.53 \text{ kw}}$

$P_{Lw} = m_w C_{pw} (T_{w2}-T_{w1})$

$T_{w1} = 74^\circ F \qquad T_{w2} = 75^\circ F$

$\underline{P_{Lw}} = 0.0764 \times 1.055 (1) = \underline{0.0806 \text{ kw}}$

Efficiency

$$\eta_t = \frac{P_t - P_{Lt}}{P_t} \times 100 = \frac{3.17-1.53}{3.17} \times 100$$

$$\underline{\eta_t} = \frac{164}{3.17} = 51.7\%$$

$$\eta_w = \frac{P_c - P_{Lw}}{P_c} \times 100 = \frac{0.976-0.0806}{0.976} \times 100$$

$$\eta_w = \frac{89.5}{0.976} = \underline{91.6\%}$$

$$H_t = \frac{P_t - P_{Lt}}{\dot{m}} = \frac{3.17 - 1.53 \text{ (kw)}}{1.35 \times 10^{-3} \text{ (lb/sec)}} \times \frac{1 \text{ BTU}}{1.055 \text{ kw-sec}}$$

$$= \frac{1.64 \times 10^3}{(1.35)(1.055)}$$

$$\underline{H_t = 1150 \text{ BTU/lbm}}$$

Voltage Gradient

$$E = \frac{V_w}{L}$$

L = Reference length = center-to-center distance

For configuration B, L = 0.5 in = 1.27 cm

$$\underline{E = \frac{16}{1.27} = 12.6 \text{ volts/cm}}$$

Mean Gas Temperature

$$T_g = T_c + \frac{H_t}{c_p}$$

c_p = 0.124 BTU/lb-°R for argon up to 18,000°R

$$T_g = 460 + 87 + \frac{1150}{0.124} = 547 + 9,270$$

$$\underline{T_g = 9820 \text{ °R}}$$

Mean Plasma Temperature

The following computations are for data taken during the Conductivity Experiment, Table III.

From Fastax Film ($Q = 0.398$ lb/sec-ft^2):

Apparent arc diameter = 22.0 mm

Apparent window height = 28.5 mm

Actual window height = 4.0 mm

Arc diameter = $4 \times \frac{22}{28.5} = 3.09$ mm

$\underline{d} = \underline{0.309 \text{ cm}}$

Conducting area = $\frac{\pi d^2}{4} = 0.075$ cm^2

Mean current density = $\frac{I}{A}$

$\underline{j} = \frac{43}{.075} = 573 \ \underline{\text{amps/cm}^2}$

$\sigma = \frac{j}{E} = \frac{573}{11.8} = 48.6$ mho/cm

From Ref 4:174,

for $\sigma = 48.6$ mho/cm

$T = \underline{12,500^\circ\text{K}}$

$= \underline{22,500^\circ\text{R}}$

Equivalent Heat Transfer Coefficient:

The following computations are for data taken during the Heat Transfer Comparison Experiment, Table IV.

$$h = \frac{Q\, C_p\, (T_w - T_c) + P_{Lw}/A_w}{(T_g - T_w)}$$

$Q = 0.223$ lb/sec-ft^2 $\qquad$ $A_w = 0.00615$ ft^2

$T_w = 368^\circ R$ $\qquad$ $C_p = 0.124$ BTU/lb-$^\circ R$

$T_c = 540^\circ R$ $\qquad$ $P_{Lw} = 0.0205$ kw

$T_g = 5400^\circ R$ $\qquad$ $= 0.0195$ BTU/sec

$$h = \frac{0.223 \times 0.124\ (28) + 195/615}{(4832)} \times 3600\ (\text{sec/hr})$$

$$= (0.774 \div 3.18)\ 0.745 = (3.95)\ (.745)$$

$$\underline{h} = 2.95 \approx \underline{3.0\ \text{BTU/hr-ft}^2\text{-}^\circ R}$$

Vita

Lieutenant Peter L. Tannen was born on [redacted] in [redacted], [redacted]. He attended [redacted], and graduated from there in 1953. He then attended Rensselaer Polytechnic Institute, graduating from the latter with the degree of Bachelor of Aeronautical Engineering in 1957. Lt. Tannen was called to active duty in 1957 and served as an Aircraft Maintenance Officer at Harlingen Air Force Base, Texas until 1960. In August 1960 he entered the Graduate Astronautics program at the Air Force Institute of Technology, and graduated in August 1962.

Lt. Tannen is an associate member of the I.A.S. and a member of Sigma Gamma Tau and Phi Sigma Kappa.

This thesis was typed by Mrs. Olga A. Heasler.

UNCLASSIFIED